Response to editor comment

By Huan Yu, hyu@nusit.edu.cn

We revised the paper to address the concerns of editor.

1. Please make saturation ratio equations for both SA and ELVOC simultaneously and look how the particle can grow.

Previously, we did not subtract H_2SO_4 growth rate (GR_{H2SO4}) from the measured Growth Rate. This is because we didn’t measure H_2SO_4 vapor with any instrument.

Now we calculate GR_{H2SO4} from H_2SO_4 proxy (Mikkonen et al. 2011 equation).

$$GR_{H2SO4} = \frac{\gamma}{2\rho_{v,H2SO4}}\left(1+\frac{D_{v,H2SO4}}{D_p}\right)^2\left(\frac{8kT}{\pi}\right)^{\frac{1}{2}}\left(\frac{1}{m_p}+\frac{1}{m_{v,H2SO4}}\right)^{\frac{1}{2}} m_{v,H2SO4}\, C_{H2SO4} \quad \text{Eq.1}$$

All parameters in eq.1 are from Nieminen et al. 2010 for H_2SO_4.

Here H_2SO_4 surface concentration over particles is set to zero, i.e., gaseous SA is assumed to condense irreversibly into post-nucleation particles (i.e. >1.7 nm). This is because ammonia, amines, and ELVOC will neutralize or stabilize H_2SO_4.

Then $GR_{elvoc} = GR_{measure} - GR_{H2SO4}$. Eq.2

The corrected GR_{elvoc}, as well as GR_{H2SO4}, are again shown in Fig S2.

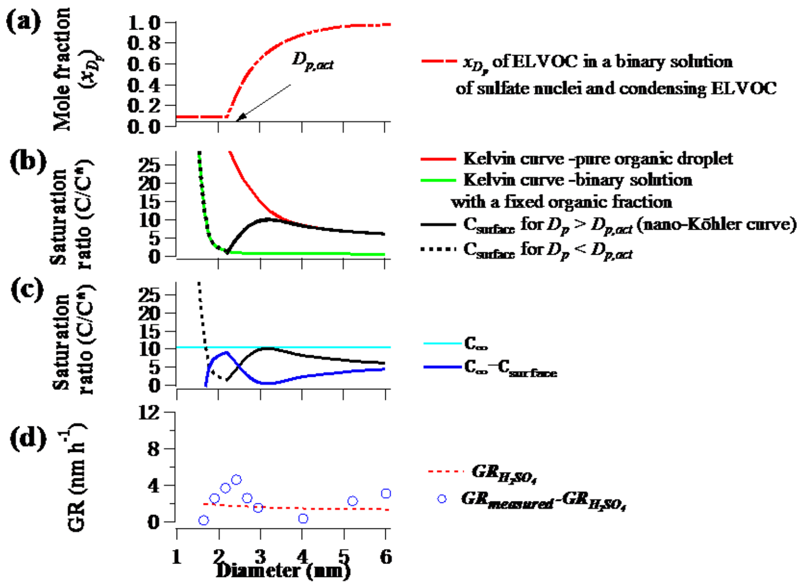

Fig S2.

From Fig S2d, We can find: 1. The varying trend of GR_{elvoc} is the same as $GR_{measure}$. Our arguments in last email still make sense. 2. H_2SO_4 can not explain all of the $GR_{measure}$. GR_{H2SO4} is monotonically decreasing and smaller than $GR_{measure}$.

After subtracting H_2SO_4, ELVOC is fitted using the equation we shown in last email:

$$GR_{elvoc} = \frac{\gamma}{2\rho_{v,elvoc}}\left(1+\frac{D_{v,elvoc}}{D_p}\right)^2\left(\frac{8kT}{\pi}\right)^{\frac{1}{2}}\left(\frac{1}{m_p}+\frac{1}{m_{v,elvoc}}\right)^{\frac{1}{2}} m_{v,elvoc}\left(C_{elvoc}-C_{surface}\right) \qquad \text{eq.3}$$

where $C_{surface} = C^*_{elvoc}\ \exp\left(\frac{4\sigma v}{kTD_p}\right) x_{D_p}$

$$x_{D_p} = \begin{cases} x_0 & , \quad D_p < D_{p,act} \\ x_0 + \dfrac{(D_p^3 - D_{p,act}^3)/v_{elvoc}}{(D_p^3 - D_{p,act}^3)/v_{elvoc} + D_{p,act}^3/v_{sulfate}}, & \quad D_p \geq D_{p,act} \end{cases}$$

where only x_0 , C_{elvoc} , and C^*_{elvoc} are free parameters and is fitted using measured GR_{elvoc} . x_0 is fitted to range from 0.07 to 0.42 for all the 8 events in the manuscript. C_{elvoc} , and C^*_{elvoc} are shown in Table 1 of the manuscript. C_{elvoc} decreases to 63% to 92% of the values without H_2SO_4 substraction.

Figure 9 is revised according, to show the corrected GR_{elvoc} and fitting curves.

2. Also, please, take into account that both SA and ELVOC concentrations are changing as a function of time.

In Fig S2, the growth rates and ELVOC concentration are for a group of particles with different size at the same instant in time. We are not tracking the same particle with size evolving as a function of time.

This is because GR calculated by our method is not from appearance time method tracking a banana contour.

Our method calculates the GR of different sizes at the same instant in time (like Kuang et al. 2012 ACP paper).

For an instant in time, if the particle composition is like what we shown in Fig S2a, we get an instant GR_{elvoc} and C_{elvoc} with Eq. 3. Then in the next time step, the particle composition changed, so did GR_{elvoc} and C_{elvoc} .

3. On the other hand, please, revisit your observational data, since I think that it might be too difficult to observe local maximas and minimas in so short time windows.

We agree with you that, using appearance time method ($GR_{H2SO4} = \frac{Dp2-Dp1}{t2-t1}$), it is not realistic to observe local maxima/minima, for such small D_p intervals and short time windows.

So we used $\frac{\mathrm{d}N(D_{p1},D_{p2},\mathrm{t})}{\mathrm{dt}} = J(D_{p1},\mathrm{t}) - J(D_{p2},\mathrm{t}) - \mathrm{CoagSnk}(D_{p1},D_{p2},\mathrm{t}) + \mathrm{CoagSrc}(D_{p1},D_{p2},\mathrm{t})$

For every 4 minutes (PSM scanning cycle), we got a $J(D_{p1},\mathrm{t})$.

Then $GR(D_p,\mathrm{t}) = J(D_{p1},\mathrm{t})/\mathrm{n}(D_{p1},\mathrm{t})$

In this way, we did not rely on short $t2-t1$ and $Dp2-Dp1$, thus it is possible to obtain GR for different size. Therefore, our GR is for an instant in time, not for a NPF growing period.

In the manuscript Section 2.3 and 3.3 we have explained this.

Nucleation and growth of sub-3 nm particles in the polluted urban atmosphere of a megacity in China

Huan Yu[1,2,*], Luyu Zhou[1], Liang Dai[1], Wenchao Shen[1], Jun Zheng[1,2], Yan Ma[1,2], Mindong Chen[1,2]

1. School of Environmental Science and Engineering, Nanjing University of Information Science and Technology, Nanjing, China

2. Collaborative Innovation Center of Atmospheric Environment and Equipment Technology, Nanjing University of Information Science and Technology, Nanjing, China

Corresponding authors: hyu@nuist.edu.cn

Abstract

Particle size distribution down to 1.4 nm was measured in the urban atmosphere of Nanjing, China in spring, summer and winter during 2014-2015. Sub-3 nm particle event, which is equivalent to nucleation event, occurred on 42 out of total 90 observation days, but new particles could grow to cloud condensation nuclei (CCN)-active sizes on only 9 days. In summer, infrequent nucleation was limited by both unfavorable meteorological conditions (high temperature and RH) and reduced anthropogenic precursor availability due to strict emission control measures during the 2014 Youth Olympic Games in Nanjing. The limiting factors for nucleation in winter and spring were meteorological conditions (radiation, temperature, and RH) and condensation sink, but for the further growth of sub-3 nm particles to CCN-active sizes, anthropogenic precursors again became limiting factors. Nucleation events were strong in the polluted urban atmosphere. Initial $J_{1.4}$ at the onset and peak $J_{1.4}$ at the noontime could be up to 2.1×10^{2} cm^{-3} s^{-1} and 2.5×10^{3} cm^{-3} s^{-1}, respectively, during the 8 nucleation events selected from different seasons. Time-dependent $J_{1.4}$ usually showed good linear correlations with a sulfuric acid proxy for every single event (R^2 = 0.56 - 0.86, excluding a day with significant nocturnal nucleation), but the correlation among all the 8 events deteriorated (R^2 = 0.17) due to temperature or season change. We observed that new particle growth rate did not increase monotonically with particle size, but had a local maximum up to 25 nm h^{-1} between 1-3 nm. The growth rate behavior was interpreted in this study as the solvation effect of organic activating vapor in newly formed inorganic nuclei.

1. Introduction

New particle formation (NPF) is an important source of secondary aerosols in the atmosphere (Kulmala et al., 2004a). Field studies and model simulations have consistently shown that NPF can enhance cloud condensation nuclei (CCN) concentrations and contribute significantly to the global CCN production (Wiedensohler et al., 2009; Yue et al., 2011; Spracklen et al., 2008; Pierce and Adams, 2009; Merikanto, 2009; Yu and Luo, 2009; Matsui et al. 2013). NPF is a two-stage process consisting of formation of clusters and subsequent growth to detectable sizes (Kulmala et al., 2000). Recently, chamber experiments have made substantial progress in revealing the fundamental processes involved in particle nucleation and growth (Kirkby et al., 2011; Almeida et al., 2013; Schobesberger et al., 2013; Riccobono et al., 2014; Ehn et al., 2014; Kürten et al., 2014). However, consistent theories are still under investigation to quantify the processes physically, chemically, and dynamically (Kulmala et al., 2013, 2014). For example, the identity and physico-chemical properties of assisting vapors other than sulfuric acid (H_2SO_4) are uncertain so far. It is also uncertain what mechanisms allow the assisting vapors to overcome strong Kelvin effect over sub-3 nm particles. Existing mechanisms include condensation of extremely low volatility organic compounds (Ehn et al., 2014), nano-Köhler activation (Kulmala et al., 2004b), heterogeneous chemical reactions (Zhang and Wexler, 2002), heterogeneous nucleation (Wang et al., 2013), and adsorption of organics on cluster surface (Wang and Wexler, 2013). However, the relative importance of various mechanisms is unknown.

Direct measurements of size- and time dependent nucleation rate and growth rate in sub-3 nm size range are important to constrain the relative contributions from different mechanisms and precursors. Such measurements are also important to evaluate the survival probability of new particle to CCN-active sizes (~100 nm for soluble particles at 0.2% super saturation, Pierce and Adams, 2009) and to reveal the limiting factors in the process. Recently, a series of new instruments have been developed to measure sub-3 nm aerosol number concentration and chemical composition, such as condensation particle counters (e.g., PSM, DEG-SMPS, Jiang et al., 2011a; Sipila et al., 2009; Vanhanen et al., 2011), ion spectrometers (e.g., NAIS, Asmi et al., 2009), and mass spectrometers (e.g., Cluster-CIMS, APi-TOF, CI-APi-TOF, Jokinen et al., 2012; Junninen et al., 2010; Zhao et al., 2010). Kuang et al. (2012) developed a de-coupling method to measure size- and time dependent growth rates of sub-5 nm particles. Their results at two urban sites in U.S.A showed that size-resolved growth rates increased approximately linearly with particle size from 1 to 5 nm.

Similar results were also observed in the Boreal forest (Kulmala et al., 2013; Lehtipalo et al., 2014). Based on growth rates measured below 2 nm, Kulmala et al. (2013) identified three separate size regimes, which were dominated by different key gas to particle conversion processes.

The relative contribution of different precursors and mechanisms to the nucleation and growth of 1-3 nm particles may vary greatly with atmospheric conditions (Riipinen et al., 2012). Therefore, sub-3 nm particle measurements in a variety of atmospheric conditions, e.g., remote or urban atmosphere, biogenic- or anthropogenic emission dominated areas, are immensely valuable. Unfortunately, such data are very sparse until now (Jiang et al., 2011b; Kuang et al., 2012; Kulmala et al., 2013; Lehtipalo et al., 2009, 2010, 2011; Yu et al., 2014a, b). China is suffering from severe atmospheric particulate matter pollution in recent years (Chan and Yao, 2008; Yue et al., 2011). To the best of our knowledge, only two studies were conducted in China to measure the occurrence of new particles down to ~1 nm. In these two studies, air ions (Herrmann et al., 2014) or neutral particles (Xiao et al., 2015) were measured by AIS or PSM in two urban locations of Yangtze River Delta region. Both studies were conducted in the winter season.

Here we reported the nucleation and growth of sub-3 nm particles in the urban atmosphere of Nanjing, China on arbitrarily selected observation days in spring, summer and winter of 2014-2015. Our aim was to (1) provide new information about the initial steps of NPF based on size- and time resolved nucleation rate and growth rate measurements, and (2) find possible limiting factors behind the seasonal and diurnal variations of nucleation events in the polluted urban atmosphere.

2. Methodology

2.1 Field measurements

Nanjing is the second largest megacity after Shanghai in the Yangtze River Delta (YRD) region of China (Chan and Yao, 2008). The YRD city cluster, covering 2.1 $\times 10^5$ km^2 land with 170 million residents, is one of the most populated and industrialized regions in China. Field measurement was conducted from the third floor (15m above the ground level) of an academic building beside a Chinese national meteorology observatory facility in NUIST campus (32.20^o N, 118.71^o E, symbol ① in Figure 1). The sampling was carried out during the months of May (May 10-30, 2014), June (June 1-15, 2014), December (December 24-31, 2014), February (February 16-22, 2015), and March (March 1-7, 2015). Total 58 measurement days were arbitrarily selected to represent spring, early summer and winter seasons, but to avoid any rain-event.

As part of an intensive summer campaign (12 August-12 September 2014), the summer measurement was conducted at a local governmental meteorology observatory platform (32.06^{o}N, 118.70^{o}E) that is 14km south to the NUIST site (② in Figure 1). The instruments were housed in an air conditioned trailer, using exactly the same sampling inlets as the NUIST site. The main aim of the summer campaign was to understand the effects of regional emission control measures during the 2014 Young Olympic Games (August 1-September 15) on air quality. Because the two sites locate within the same urban air shed, the measurement provided an opportunity to study seasonal variation of nucleation and its relationship with meteorological variables and gaseous precursors.

Sub-3 nm clusters/particles (hereafter referred as particles) were measured with a nano condensation nucleus counter system (nCNC) consisting of a Particle Size Magnifier (PSM model A10, Airmodus Oy, Finland) and a butanol Condensation Particle Counter (model A20, Airmodus Oy, Finland). During the measurement, an ambient air flow of 14 standard liters per minute (slpm) was drawn into building room or trailer via a 72 cm long and 1.0 cm I.D diameter stainless steel (SS) tube, which was extended outside the room/trailer horizontally. PSM then sampled a split flow of 2.5 slpm via a SS T-union. The design of the inlet tubing (length and air flow rate) was to minimize the transport loss of nano particles. The size dependent transport survival ratios of sub-3 nm particles in the inlet tubing was estimated (67 %-86 % for 1.4-3.0 nm) and corrected using a particle loss calculator tool (von der Weiden et al., 2009).

PSM was operated in a continuous scanning mode with a cycle of 240 steps between saturator flow rates of 0.1 and 1.0 slpm within 240 seconds. The particle cut-off sizes of the nCNC varied with saturation ratios in the saturator (Vanhanen et al., 2011). A step-wise method was used to invert raw scanning data to size spectrum (time resolution: 4 minutes) of sub-3 nm particles, which were classified evenly into 6 size bins, i.e. 1.4-1.6, 1.6-1.9, 1.9-2.2, 2.2-2.4, 2.4-2.7, and 2.7-3.0 nm. The inverted particle number concentrations in the 6 bins were referred as $N_{1.5}$, $N_{1.8}$, $N_{2.0}$, $N_{2.3}$, $N_{2.6}$ and $N_{2.8}$, using mean values of upper and lower size boundaries in each bin. The step-wise method was described in detail by Lehtipalo et al. (2014).

Particle size distributions in the range from 3 - 750 nm were obtained by integrating two scanning mobility particle spectrometers (SMPS) with a nano-SMPS (a TSI differential mobility analyzer DMA3085 and a condensation particle counter CPC3776; scanning range: 3 - 64 nm) and a long-SMPS (TSI DMA3081 and CPC3775; scanning range: 64 - 750 nm). During the summer campaign, only the long-SMPS was operated to scan particles from 8 - 350 nm. Scanning cycles of both SMPS systems were 4 minutes, in order to synchronize with the nCNC. The SMPSs sampled ambient air from a separate sampling inlet. The inlet was a 129 cm long and 1.0 cm I.D horizontally-oriented SS tube with an air flow of 14 slpm. The transport loss of particles in the SMPS inlets was corrected using size dependent survival ratios of 85-100% for particles > 3 nm.

Sulfur dioxide (SO_2), ozone (O_3), carbon monoxide (CO) and nitrogen oxides (NO and NO_2) concentrations were measured every 1 minute with Thermo Environmental Instruments (model 43i-TLE, 49i, 48i, and 42i, respectively). When gaseous SO_2, O_3, NO_2 and CO data were not available, hourly SO_2, O_3, NO_2 and CO were obtained from nearby local Environmental Protection Agency (EPA) monitoring station. $PM_{2.5}$ was monitored with Thermo Scientific TEOM 1405. Meteorological variables including wind speed, wind direction, relative humidity (RH), temperature and solar radiation flux were recorded every 1 hour during the measurement periods. Mean concentrations of $PM_{2.5}$, SO_2, and O_3 were 79 $\mu g\ m^{-3}$, 10 ppbv and 48 ppbv, respective, during the whole measurement period. Therefore, we regard our measurement environment as a polluted urban atmosphere.

2.2 Nucleation event and growth patterns

A criterion was set to determine whether the nCNC detected sub-3nm particles in the atmosphere. The criterion was that total particle concentration reading followed the supersaturation scanning cycle of PSM so that the highest concentrations were measured at lowest cut-off sizes (see also Figure 2 in Lehtipalo et al., 2014). However, it was possible in the step-wise inversion method that the number concentration fluctuation of > 3 nm particles within a 4-min scanning cycle was wrongly inverted to sub-3 nm particles even when sub-3 nm particles actually did not exist according to the above criterion. As a result, the step-wise inversion method always reported a background sub-3 nm particle concentration ($N_{sub\text{-}3}$, i.e. the sum of $N_{1.5}$, $N_{1.8}$, $N_{2.0}$, $N_{2.3}$, $N_{2.6}$ and $N_{2.8}$) of 0.5×10^3 - 2×10^3 cm^{-3} in the nighttime and 3×10^3 - 8×10^3 cm^{-3} in the daytime. Similar background levels of sub-3 nm particles during non-NPF periods were also reported by other studies that used the nCNC (Kulmala et al., 2013; Lehtipalo et al., 2014; Xiao et al., 2015). Following their procedures, we did not attempt to subtract this background from $N_{sub\text{-}3}$ reported in this study.

We defined sub-3 nm particle event as sub-3 nm particle occurrence with $N_{sub\text{-}3}$ higher than background level persisting for longer than 1 h in the atmosphere. In this study, we used sub-3 nm particle event as an approximate measure of nucleation event. This is because (1) there was an approximately positive linear correlation between $N_{sub\text{-}3}$ and nucleation rate ($J_{1.4}$ in this study, see next section) with R^2 of 0.94 (Figure 2), and (2) $N_{sub\text{-}3}$ calculation needs only nCNC scanning data and was thus more readily available than $J_{1.4}$ calculation which needs both nCNC and SMPS scanning data. Similar definition has been discussed in our previous studies (Yu et al., 2014a, b). Apparently, a sub-3 nm particle event did not necessarily lead to an NPF event always, but it indicated the intensity and frequency of nucleation in the atmosphere. One focus in this work was to investigate the characteristics of sub-3 nm particle event.

Particle growth after nucleation is crucial to determine if nucleated particles could grow to CCN-active sizes. We identified two growth patterns according to size spectrum characteristics in sub-3 nm size range (Figure 3). In a Type A event (Figure 3a or b), size distribution n(D_p, t) was higher at smaller sizes (e.g., 1.4–1.6 nm) than n(D_p, t) at larger sizes (e.g., 2.7–3.0 nm). The size spectrum below 3 nm thus looked like a “volcano”. In a Type B event (Figure 3c or d), n(D_p, t) was lower at smaller sizes than n(D_p, t) at larger sizes (“up-side-down volcano”). For the size range > 3 nm, depending on whether a banana-shape growth was seen, we further defined Type A1/A2 and Type B1/B2 events: particles eventually grew to CCN-active sizes in Type A1 and B1 events, while in Type A2 and B2 events banana-shape particle growth to CCN-active sizes was not seen. Therefore, Type A1 and B1 events were equivalent to conventional NPF events based on either DMPS or SMPS measurements.

Type B size distribution was more unusual since n(D_p, t) of small particles were less than n(D_p, t) of large particles in the sub-3 nm size range. We excluded the possibility of deteriorated nCNC detection efficiencies for small particles due to high particle loading in the sample air. This is because total number concentrations of nCNC during our measurements never approached nCNC upper concentration limit 4×10^5 cm^{-3}, especially in the early stage of nucleation when total particle concentration was rather low. Our nCNC was also calibrated periodically using H_2SO_4-H_2O particles in a laboratory flow tube to ensure the detection efficiency of the nCNC. The different chemical composition of atmospheric particles could be another factor of lower detection efficiencies. It is well known that organic substances activate less readily in diethylene glycol (e.g. Kangasluoma et al. 2014). However, it is accepted in general that larger particles have higher mass fraction of organics than smaller particles in a NPF process. If organic substances activate less readily in DEG, it should be even more difficult to activate larger particles than smaller particles. Therefore, the increasing n(D_p) with D_p (i.e. upside down volcano) could not be simply due to lower detection efficiency of organic substances.

2.3 Formation rate and growth rate calculations with a simplified GDE method

Conventional appearance time method determined growth rates (hereafter, *GR*) during the initial period of NPF by finding the time steps when newly-formed particles appeared at certain size bins and calculating the *GR* from the time differences between successive size bins (Kulmala et al., 2012; Lehtipalo et al., 2014). This method was often not applicable to the NPF event with high *GR* below 3 nm, e.g., 0.3 nm/4 min (i.e. 4.5 nm h^{-1}) with size intervals 0.3 nm and scanning time intervals 4 minutes in our measurements. Furthermore, sub-3 nm particles were often generated persistently throughout the daytime period. Maximum concentrations in the sub-3 nm size bins could appear around noontime, which is a few hours later than the onset of nucleation. Therefore, we were not able to pinpoint correctly maximum or 50% maximum concentrations at the onset of nucleation.

The rapid growth of small particles in the urban atmosphere was the motivation that we used an alternative method to calculate growth rate and formation rate. Here, we analyzed 8 events (listed in Table 1, including both Type A1/A2 and B1/B2 events) in detail, for which complete size spectra from 1.4 - 750 nm were available without distorted, broken or noisy data. Total 8 size bins were classified: 6 evenly-divided size bins in sub-3 nm and 2 size bins in 3-30 nm (3-10 and 10-30 nm). For an aerosol population that is growing through simultaneous condensation and coagulation, aerosol general dynamic equation (GDE) describes the evolution of number concentration in a size bin between particle diameters D_{p1} and D_{p2} ($D_{p2} > D_{p1}$) as:

$$\frac{\mathrm{d}N(D_{p1},D_{p2},\mathrm{t})}{\mathrm{dt}} = J(D_{p1},\mathrm{t}) - J(D_{p2},\mathrm{t}) - \mathrm{CoagSnk}(D_{p1},D_{p2},\mathrm{t}) + \mathrm{CoagSrc}(D_{p1},D_{p2},\mathrm{t}) \qquad (1)$$

where $N\left(D_{p1}, D_{p2}, \mathrm{t}\right)$ is the number concentration from D_{p1} to D_{p2}, inverted from nCNC or SMPS scanning data. J is condensational growth flux (i.e. particle formation rate) across the lower ($D_{p,1}$) or upper ($D_{p,2}$) boundaries of a size bin. In the first size bin of 1.4-1.6 nm, $J(1.4\ \mathrm{nm}, \mathrm{t})$, or simply $J_{1.4}$, is the unknown formation rate of the smallest particles that we measured.

$\mathrm{CoagSnk}\left(\mathrm{D_{p1}}, \mathrm{D_{p2}}, \mathrm{t}\right)$ and $\mathrm{CoagSrc}\left(\mathrm{D_{p1}}, \mathrm{D_{p2}}, \mathrm{t}\right)$ are the sink and source terms defining the coagulation out of and into the size bin between D_{p1} and D_{p2}. Assuming bin k has lower boundary $D_{p,1}$ and upper boundary $D_{p,2}$,

$$\mathrm{CoagSnk}\left(\mathrm{D_{p1}}, \mathrm{D_{p2}}, \mathrm{t}\right) = \mathrm{N}(\mathrm{k}, \mathrm{t}) \sum_{\mathrm{i}=1}^{98} (1 - \theta_{\mathrm{k,i,k}}) \mathrm{K_{k,i}}\, \mathrm{N}(\mathrm{i}, \mathrm{t}) \tag{2}$$

$$\mathrm{CoagSrc}\left(\mathrm{D_{p1}}, \mathrm{D_{p2}}, \mathrm{t}\right) = \frac{1}{2} \sum_{\mathrm{i}=1}^{\mathrm{k}-1} \sum_{\mathrm{j}=1}^{\mathrm{k}-1} \theta_{\mathrm{i,j,k}}\, \mathrm{K_{i,j}} \mathrm{N}(\mathrm{j}, \mathrm{t}) \mathrm{N}(\mathrm{i}, \mathrm{t}) \tag{3}$$

Here $\mathrm{N}(\mathrm{i}, \mathrm{t})$ is number concentration of bin i. $\mathrm{K_{i,j}}$ is coagulation kernel for a collision between particles from bins i and j. Probability coefficient $\theta_{\mathrm{i,j,k}} = 1$, if the volume sum of two coagulating particles ($\mathrm{v_i} + \mathrm{v_j}$, here the volume is calculated from the center diameter of a bin) is within the volume boundaries of bin k. otherwise $\theta_{\mathrm{i,j,k}} = 0$. The particle coagulation of total 98 bins was considered, but the coagulation terms were only needed to be calculated for the smallest 8 bins from 1.4 to 30 nm. According to our calculation, $\mathrm{CoagSrc}\left(\mathrm{D_{p1}}, \mathrm{D_{p2}}, \mathrm{t}\right)$ accounted for only 0 - 0.8 % of the total particle flux into a bin (i.e. $\mathrm{CoagSrc}\left(\mathrm{D_{p1}}, \mathrm{D_{p2}}, \mathrm{t}\right) + J\left(D_{p1}, \mathrm{t}\right)$) in the sub-3 nm size range. This implied that self coagulation played a negligible role and most of the production flux into a bin is due to condensational growth from gas molecules.

The GDE here is the same as the Eq. 1 by Kuang et al. (2012). In their method, gaseous H_2SO_4 was measured simultaneously and a constant $GR(D_p, \mathrm{t})$ / $GR_{H2SO4}(D_p,\mathrm{t})$ ratio at a given size over time was assumed. Their $GR(D_p, t)$ was then solved by fitting the GDE to the measured size distributions. In our study, however, we did not measure gaseous H_2SO_4. Instead, $J(30\ \mathrm{nm}, \mathrm{t})$ in the largest size bin, which is the condensational growth flux out of 30 nm, was set to zero. This simplification was valid in the four Type A2/B2 events when particles never grew to > 30 nm (March 4, February 19, May 20 and May 16). In the rest four Type A1/B1 events (February 18, December 27, May 15, and August 15), this was also valid during the early NPF period when particles did not grow out of 30 nm and during the late NPF period when particles grew out of 30 nm completely. During the middle period of events (usually around 11:00 AM-14:00 PM), $J(30\ \mathrm{nm}, \mathrm{t})$ was underestimated and thus $J_{1.4}$ could be regarded as a lower estimate. In the four Type A2/B2 events, our calculation showed that J_{10} was only 0-4% of $J_{1.4}$. Xiao et al. (2015) and Kulmala et al. (2013) measured both $J_{1.5}$ and J_3 using appearance time method. Their J_3 was less than 7% of $J_{1.5}$. Furthermore, $J_{30}/J_{1.4}$ ratio should be even smaller than $J_{10}/J_{1.4}$ or $J_3/J_{1.5}$ ratios, considering the 8 events were carefully selected to ensure all sub-30 nm particles were grown from nucleation (not emitted directly from emission sources like vehicular engine). All these evidences supported that even if J_{30} was set to 0, $J_{1.4}$ would not be underestimated more than 7% when particles grew cross 30 nm on February 18, December 27, May 15, and August 15.

Equation 1 requires the balance of condensational growth (J), coagulation terms (CoagSnk and CoagSrc) and the changing rate of particle number concentration (dN/dt). Using Eq. (1) we can therefore calculate the nucleation rate $J(1.4\ \mathrm{nm}, \mathrm{t})$ and formation rates $J(D_p, \mathrm{t})$ across all size bin boundaries from 1.6 to 10 nm. After the formation rates $J(D_p, \mathrm{t})$ were obtained, $GR(D_p, \mathrm{t})$ was calculated from $J(D_p, \mathrm{t})/\mathrm{n}(D_p, \mathrm{t})$, where $\mathrm{n}(D_p, \mathrm{t})$ is size distribution calculated as $\mathrm{n}(D_p, \mathrm{t}) = \frac{\mathrm{d}N(\mathrm{t})}{\mathrm{d}D_p}$

for each size bin. On the other hand, the appearance time method could still be applied to (1) the size range of > 3 nm where size intervals were large (2-6 nm), and (2) the size range of < 3 nm when *GR* was small. The results from appearance time method will also be showed in the next section.

3. Results and discussion

Section 3.1, sections 3.2-3.4 and section 3.5 were organized, respectively, to address the following 3 issues: (1) seasonal variation, diurnal variation and limiting factors of nucleation event (represented by sub-3 nm particle event) in the polluted urban atmosphere, (2) time- and size dependent nucleation rate and growth rate of sub-3 nm particles, and their implications for nucleation and growth mechanisms, (3) Inhibited particle growth to CCN-active sizes in strong nucleation events of Type B2.

3.1 Seasonal and diurnal variations of nucleation event

As seen from Figure 2, there was an approximate linear correlation between $N_{sub\text{-}3}$ and $J_{1.4}$ with the slope of $N_{sub-3}/J_{1.4}$ equal to ~160. This seemed to suggest that the average residence time of new particles in the sub-3 nm size range was 160 seconds before they were scavenged due to coagulation or grew out of 3 nm. The sub-3 nm particles observed at the present work were thus formed in situ in the urban atmosphere and not likely to be carried-over by air transport. In this section we used sub-3 nm particle event as an approximate measure of nucleation.

We observed significant seasonal characteristics of nucleation event (Figure 4). Nucleation was rare and weak in summer, while it was commonly observed in all other seasons. During our measurements from 2014 to 2015, nucleation events occurred on 81% of all spring observation days (May 2014), 53% in early summer (June 2014), 10% in summer (August and September 2014), and 64% in winter (December 2014, February and March 2015). We compared intensity ($N_{sub\text{-}3}$) and frequency of nucleation events, as well as meteorological variables (temperature, RH, wind speed, and solar radiation flux) and gaseous pollutants (SO_2, NO_2, CO and O_3) for spring, summer and winter seasons. June was not shown in Figure 4 for comparison, because it was a transit season from spring (May) to summer (August and September). The data were first averaged over the entire event period for each event; and we then used event-averaged data to create box and whistler plots for the 3 seasons. $PM_{2.5}$ was used here as a surrogate of condensational sink (*CS*), because of the more ready availability of $PM_{2.5}$ data than SMPS data.

As shown in Figure 4, nucleation in summer was characterized by lowest frequency, lowest $N_{sub\text{-}3}$ (2.2×10^4 cm^{-3}), and short nucleation period (only 1-2 hours). Strict emission control measures during the 2014 Youth Olympic Games resulted in relatively low $PM_{2.5}$ level (32 ± 8 $\mu g\ m^{-3}$), which should favor nucleation. However, relatively low SO_2 concentration (1.4 ± 0.6 ppbv), high temperature (26 ± 2 ^oC), and high RH (74.3 ± 4.2 %) might not be in favor of nucleation. A simple H_2SO_4 proxy (Radiation$\times SO_2/PM_{2.5}$) indicated that summer H_2SO_4 concentration was likely to be the lowest among the 3 seasons, which could explain low nucleation intensity/frequency.

We further examined diurnal variations of $N_{sub\text{-}3}$ and other variables on event and non-event days in winter (Figure 5). Because nucleation in winter was characterized by Type B event (“up-side-down volcano” below 3 nm), event days were further divided to Type B1 and Type B2 events depending on whether banana-shape particle growth was seen. The difference between Type

B1 and B2 will be discussed later in Section 3.5. During the non-event days, $N_{sub\text{-}3}$ ranged from 2.4×10^3 cm^{-3} in the night to 8.0×10^3 in the day, which was close to background levels. During the event days, $N_{sub\text{-}3}$ in the night was close to that of non-event days, but could reach 8×10^4 - 20×10^4 cm^{-3} in the middle of the day. This was more than 10 times higher than those on the non-event days. From Figure 5 we can see that non-event day had higher concentrations of anthropogenic precursors (indicated by SO_2, NO_2, and CO), but nucleation seemed to be limited by higher pre-existing particle surface area (indicated by $PM_{2.5}$), higher temperature and RH, and lower radiation flux. Photochemistry indicators O_3 was also lower during non-event days.

Nucleation in spring was characterized by highest frequency (81%) among all seasons. Highest gaseous pollutant concentration of (H_2SO_4 proxy, SO_2, NO_2, CO and O_3) and radiation seemed to the favorable factors to explain this. However, $N_{sub\text{-}3}$ in spring (3.3×10^4 cm^{-3}) was much lower than that in winter (11.2×10^4 cm^{-3}). Unfavorable factors included high pre-existing particle surface area ($PM_{2.5}$: 112 ± 68 μg m^{-3}) and high temperature (27 ± 4 ^{o}C) in spring. Integrating the above seasonal and diurnal variation information in Figure 4 and Figure 5, we tentatively identified that the limiting factors for nucleation in our urban atmosphere were (1) radiation, temperature, RH and *CS* in winter and spring, and (2) temperature, RH and available gaseous precursors in summer.

Out of total 90 measurement days, March 4, 2015 in winter was the only day that we observed significant nocturnal nucleation. Sunrise and sunset were at 6:29 AM and 18:00 PM local time on March 4, but nucleation were observed persistently from 4:00 AM - 20:00 PM. $N_{sub\text{-}3}$ increased from 3.5×10^3 cm^{-3} at 4:00 AM to 6.3×10^4 cm^{-3} before sunrise. During 10:00-11:00 AM, peak $N_{sub\text{-}3}$ reached 3×10^4 cm^{-3}, 3 times higher than the average of all other event days in winter. Apparently, nocturnal nucleation on March 4 could not be explained as carry-over of daytime particles nor being associated with photochemistry. This implied the existence of certain dark nucleation source. There are a number of observations that have also shown nighttime particle formation events in various atmospheric conditions (Junninen et al., 2008; Lehtipalo et al., 2011; Lee et al., 2008; Ortega et al., 2009, 2012; Russell et al., 2007; Suni et al., 2008; Svenningsson et al., 2008; Yu et al., 2014), but the mechanisms behind the nocturnal nucleation are yet still highly speculative. With our instrument capability in this work, we could not deduce any valuable information on the nocturnal nucleation mechanism, except that we found the air mass on 04 March was relatively clean (both *CS* and gases, mean *CS*: 0.15 s^{-1}), and temperature and RH (mean: 4.4^{o}C and 33%) were favorable for nucleation.

3.2 Size- and time dependent formation rates of sub-3 nm particles

We observed 23 Type A events and 9 Type B events during the measurements. The different size distribution patterns (Figure 3) were probably linked to the mechanism or intensity of nucleation and growth. To address this issue, we first compared the formation rates and growth rates in two types of events. Formation rates J of 1.4, 1.6, 1.9, 2.2, 2.4, 2.7 and 3.0 nm particles were shown in Figure 6 (upper panels) for typical Type A and Type B events. It is obvious that $J_{1.4}$ was much higher on February 18 (Type B) than that on May 15 (Type A). A clear time dependence of J was observed. For example, $J_{1.4}$ was 60 cm^{-3} s^{-1} at the onset of the nucleation event on May 15 and increased to 300 cm^{-3}s^{-1} in the middle of the day. In the type B event on February 19, the initial and peak $J_{1.4}$ were 2.1×10^{2} and 1.2×10^{3} cm^{-3}s^{-1} respectively. Therefore, our method provided more information of nucleation than conventional calculation methods that usually showed only an averaged J at the onset of a nucleation event. Our method was also different from Kulmala et al. (2013). Their time-dependent formation rate on an event day was equal to size distribution n(D_p,t) times a constant growth rate at the onset of the event obtained with the appearance time method.

The diurnal variation of J implied that nucleation was probably linked to sunlight induced photochemistry. We calculated the correlations between $J_{1.4}$ and an H_2SO_4 proxy for the 8 events of our interest. The H_2SO_4 proxy was calculated following $[\mathrm{H_2SO_4}] = 8.21 \times 10^{-3} k \cdot Radiation \cdot [SO_2]^{0.62} \cdot (CS \cdot RH)^{-0.13}$(Eq. 8 of Mikkonen et al. 2011), where k is the temperature-dependent reaction-rate constant. Figure 7a show that good linear correlation was usually seen for every single event with R^2 ranging from 0.72 to 0.86 for 6 out of 8 events. A moderate R^2 of 0.56 was obtained for August 15. R^2 was lowest (0.34) on March 4, 2015. This is not surprising because we know March 4 was the only day with nocturnal nucleation during the measurement period. The H_2SO_4 proxy was also calculated using the derivation of Petäjä et al. (2009), which resulted in lower R^2 of log $J_{1.4}$ *vs.* log [H_2SO_4] for all 8 events. Therefore, in this study we used Mikkonen H_2SO_4 proxy, as it was derived with more comprehensive datasets than Petäjä et al. (2009). The slopes of log $J_{1.4}$ *vs.* log [H_2SO_4] were close to 1 in all events (0.82-1.17, excluding March 4), indicating activation theory can explain the nucleation mechanism in our urban atmosphere.

If data points of all the 8 events were put together, the linear correlation between H_2SO_4 proxy and $J_{1.4}$ deteriorated (slope=1.1, R^2=0.17, Figure 7b). In spite of considerable scattering, most of data points located between $J_{1.4}=10^{-4.1} \times [H_2SO_4]$ and $J_{1.4}=10^{-6.3} \times [H_2SO_4]$. An interesting finding was that the scattering of $J_{1.4}$ *vs.* [H_2SO_4] proxy among all 8 events was probably due to temperature or season change (Figure 7b). More specifically, with the same level of H_2SO_4 proxy, $J_{1.4}$ was higher in winter with lower temperature than in spring/summer with higher temperature. There were two possibilities behind the deteriorated linear correlation between H_2SO_4 proxy and $J_{1.4}$: (1) inaccurate H_2SO_4 proxy and (2) other varying factors in nucleation mechanism. First, it was very likely that H_2SO_4 concentrations in our polluted urban atmosphere were overestimated by the H_2SO_4 proxy of Mikkonen et al. (2011), which was based on statistic regression of historical datasets from relatively clean Europe/USA atmosphere. The extent of overestimation may vary with the levels of predictor variables (e.g., SO_2, temperature, *CS*). Mean SO_2 mixing ratios were 10.5 and 7.3 ppbv in spring/summer and winter during our measurements, respectively. These were 1 order of magnitude higher than SO_2 mixing ratios at the 6 European and USA sites (mean values: 0.23-3.4 ppbv, Mikkonen et al., 2011). Our *CS* in the 8 events was on the order of magnitude of 10^{-2} s^{-1}, again higher than 10^{-3} s^{-1} in Mikkonen et al. (2011). Mikkonen et al. (2011) had already pointed out that the predictive ability was lower for long term data due to atmospheric condition changes in different seasons.

Second, organic condensing vapor concentrations in particle growth events were higher in winter than those in spring/summer (Table 1, see Section 3.4). If the organics were also involved in nucleation, $J_{1.4}$ should be enhanced in winter. The enhancement of nucleation by organics (most likely anthropogenic organics in our urban atmosphere) could be supported by the comparison of $J_{1.4}$ dependences on H_2SO_4 between our study and the measurements in the Boreal forest: besides possible H_2SO_4 overestimation, $J_{1.4}=10^{-4.1}\times[H_2SO_4] - 10^{-6.3}\times[H_2SO_4]$ in our sites was much higher than $J_{1.5}=1.06\times10^{-7}[H_2SO_4]^{1.1}$ in Hyytiälä during active aerosol formation periods (Kulmala et al., 2013). At last, low temperature itself might enhance nucleation in winter (Brus et al., 2011) via increasing the saturation ratios of all nucleation precursors (e.g., water, H_2SO_4, organics).

3.3 Size- and time dependent growth rates of sub-3 nm particles

Particle size distribution n(D_p) and corresponding $GR(D_p)$ at an instant in time during the events were shown in Figure 6 middle and lower panels. A local minimum of n(D_p) at 2.4 nm, followed by a local maximum somewhere between 2.5 and 10 nm, was seen on May 15, 2014. Such size distribution characteristics on May 15, 2014, as well as on all other Type A event days, was also observed by Kulmala et al. (2013) in the Boreal forest (Figure 1A and S9A in their paper) and by Jiang et al. (2011b) in the urban area of Atlanta, USA (Figure 1 in their paper). We further examined the growth rates in the size range of 1-3 nm on May 15, 2014. It was shown that there was a local maximum of $GR(D_p)$ at 2.4 nm. This could explain why n(D_p) was increasing in 2.4-3 nm size range: when particle condensational flow out of a size bin was slowed down, it was possible that particles flowing into the size bin accumulated, leading to particle number increase in the bin.

We saw more unusual behaviors of n(D_p) and GR(D_p) in the Type B event on February 18 (Figure 6 right panels): $GR(D_p)$ decreased monotonically in the size range of 1.4 - 3 nm, and accordingly n(D_p) increased monotonically at the same time. A high $GR(D_p)$ of 25 nm h^{-1} was observed at 1.6 nm and $GR(D_p)$ decreased rapidly to 1.7 nm h^{-1} at ~3 nm. If we consider that $GR(D_p)$ below 1.6 nm would eventually decrease due to strong Kelvin effect of all possible precursors (H_2SO_4 or organics), the overall trend of $GR(D_p)$ in the Type B event was in fact the same as Type A:

for the smallest clusters, growth rate was small (possibly below 1 nm h^{-1}) and increased with D_p. It reached a local maximum somewhere between 1-3 nm, after which $GR(D_p)$ decreased with D_p. For a typical NPF event, $GR(D_p)$ would eventually increase again after a local minimum between 3-10 nm. The difference between the Type A event (February 18) and Type B event (May 15) was the D_p of local maximum $GR(D_p)$ (2.4 nm *vs.* 1.6 nm).

The interesting behaviors of n(D_p) and GR (D_p) in our urban atmosphere were different from the stereotyped understanding that steady-state cluster size distribution n(D_p) decreases with D_p in nucleation and GR increases monotonically with D_p in an NPF event. It should be pointed out that if we calculated the overall GR in 1.4-3 nm, $GR_{1.4\text{-}3}$ was 3.6 nm h^{-1} on May 15 and 4.4 nm h^{-1} on February 18, which were still smaller than $GR_{3\text{-}20}$ during the initial period of the events (7.7 and 6.0 nm h^{-1}, calculated using appearance time method). Table 1 showed that a faster $GR_{3\text{-}20}$ than $GR_{1.4\text{-}3}$ were quite common, except in two events on May 16 and 20 when particles did not grow beyond 3 nm. Overall, GR was still increasing with increasing D_p.

Kuang et al. (2012) had also reported a local maximum of GR at ~2.6 nm in an NPF event measured in Atlanta, USA (Figure 1b in their paper). In this study we further point out that GR could decrease monotonically with D_p in 1-3 nm range in strong nucleation events. Our GR was calculated from a simplified GDE method, however, the decease of GR in 1-3 nm size range could be easily inferred from the size spectra shown in Figure 3 or Figure 6 middle panels: for a D_{p2} that was larger than D_{p1}, particle formation rate $J(D_{p2})$ must be smaller than $J(D_{p1})$. If we observed a higher n(D_{p2}) than n(D_{p1}), $GR(D_p)$ that was equal to $J(D_p)$/n(D_p) must be smaller at D_{p2} than D_{p1}.

3.4 Growth rate due to condensing organic vapor on newly formed nuclei in sub-3 nm sizes

Apparently, the complicated growth rate behaviours in our polluted urban atmosphere can not be explained by H_2SO_4 condensation alone, not only because H_2SO_4 condensational growth rate (GR_{H2SO4}, calculated from the H_2SO_4 proxy and shown as black dashed lines in Figure 6) was smaller than the measured growth rate (GR_{meas}), but also because GR_{H2SO4} curve should follow a monotonically decreasing trend in > 1 nm sizes assuming a collision-only condensational growth without vaporization (Nieminen et al., 2010).

Nano-Köhler theory (Anttila et al., 2004; Kulmala et al., 2004b, c) suggested that when a soluble organic vapor is dissolved in newly formed nuclei of aqueous-phase sulfate at certain size between 1-3 nm, the surface organic vapor pressure is lowered and thus assists the growth of the nuclei. Here, we continued our discussion based on the nano-Köhler theory to provide an explanation of *GR* behaviours observed in our urban atmosphere. We first subtract GR_{H2SO4} from GR_{meas} to obtain the growth rate due to a condensing organic vapor (hereafter, denoted as ELVOC, extremely low volatility organic compound):

$$GR_{meas,elvoc} = GR_{meas} - GR_{H2SO4}$$

where GR_{H2SO4} is calculated from the H_2SO_4 proxy concentration $[H_2SO_4]$ following Nieminen et al. (2010),:

$$GR_{H2SO4} = \frac{\gamma}{2\rho_{v,H2SO4}}\left(1+\frac{D_{v,H2SO4}}{D_p}\right)^2\left(\frac{8kT}{\pi}\right)^{\frac{1}{2}}\left(\frac{1}{m_p}+\frac{1}{m_{v,H2SO4}}\right)^{\frac{1}{2}} m_{v,H2SO4}\;[H_2SO_4] \qquad (4)$$

and all parameters in Eq.4 are taken from Nieminen et al. (2010) for H_2SO_4.

The size-dependent growth rate due to the uptake of ELVOC was expressed as

$$GR_{elvoc} = \frac{\gamma}{2\rho_{v,elvoc}}\left(1+\frac{D_{v,elvoc}}{D_p}\right)^2\left(\frac{8kT}{\pi}\right)^{\frac{1}{2}}\left(\frac{1}{m_p}+\frac{1}{m_{v,elvoc}}\right)^{\frac{1}{2}} m_{v,elvoc}\left(C_{elvoc}-C_{surface}\right) \qquad (5)$$

where C_{elvoc} is gas-phase ELVOC concentration far from the particle. The net uptake of ELVOC is driven by the difference of C_{elvoc} and equilibrium surface concentration over the particle $C_{surface}$. $C_{surface}$ is determined by the pure component saturation vapor pressure C^{*}_{elvoc}, particle curvature $\exp\left(\frac{4\sigma v}{kTD_p}\right)$ and particle composition:

$$C_{surface} = C^{*}_{elvoc}\exp\left(\frac{4\sigma v}{kTD_p}\right)x_{D_p}$$

x_{D_p} is the mole fraction of water-soluble ELVOC in the pseudobinary solution consisting of ELVOC and the aqueous sulfate nuclei. The pseudobinary solution was treated ideal here. An example of x_{D_p} as a function of D_p was shown in Figure 8a. Nuclei activation diameter $D_{p,act}$ is the size that ELVOC fraction begins to increase significantly. For $D_p < D_{p,act}$, x_{D_p} is approximated with a fixed value (x_0). For $D_p > D_{p,act}$, x_{D_p} increases significantly with the organics being added to the sulfate core of $D_{p,act}$ size. The size dependent x_{D_p} is approximated as

$$x_{D_p} = \begin{cases} x_0 & , \quad D_p < D_{p,act} \\ x_0 + \dfrac{(D_p^3 - D_{p,act}^3)/v_{elvoc}}{(D_p^3 - D_{p,act}^3)/v_{elvoc} + D_{p,act}^3/v_{sulfate}} & , \quad D_p \geq D_{p,act} \end{cases}$$

Considering strong Kelvin effect, $C_{surface}$ decreases with increasing D_p for $D_p < D_{p,act}$ (Figure 8b dashed black line). For $D_p > D_{p,act}$, the rapidly increasing organic fraction in the small size regime of 2-3 nm raises the equilibrium $C_{surface}$ of ELVOC first. Then for 3-6 nm particles that are dominated by organics, $C_{surface}$ decreases to merge with the Kelvin curve of a pure organic droplet (red line, Figure 8b). The complete equilibrium curve of $C_{surface}$ in 1-6 nm (dashed + solid black lines) was shown in Figure 8c. The blue line represented the calculated $\mathrm{C_{elvoc}} - \mathrm{C_{surface}}$. The trend of $\mathrm{C_{elvoc}} - \mathrm{C_{surface}}$ coincided with the size dependence of the measured *GR* corrected by H_2SO_4 ($GR_{meas,elvoc}$, Figure 8d blue circle). $D_{p,act}$ corresponded to the size with local maximum $GR_{meas,elvoc}$.

We fitted GR_{elvoc} with $GR_{meas,elvoc}$ in sub-3 nm sizes at an instant in time by adjusting 3 free parameters in Eq. (5): x_0, $\mathrm{C_{elvoc}}$, and $\mathrm{C^*_{elvoc}}$. Other parameters like surface tension (0.02 N m^{-1}) and molar volume (135.5 cm^3 mol^{-1}) of ELVOC were taken from Kulmala et al. (2004b). Molecule diameter d_v (0.8 nm) and condensed-phase density ρ_v (1.5 g cm^{-3}) of ELVOC were taken from Ehn et al. (2014). Uptake coefficient γ was calculated following Nieminen et al. (2010). The fitting results in Figure 9 showed that the dependence of $GR_{meas,elvoc}$ on D_p below 3 nm could be well reproduced by Eq. (5) for both Type A and Type B events. Free parameter x_0 determined the magnitude of the dashed black line in Figure 8b. x_0 was fitted to be 0.07-0.42 for the 8 events. $\mathrm{C_\infty}$ was sensitive to the local maximum $GR_{meas,elvoc}$ at the $D_{p,act}$. $\mathrm{C_{elvoc}}$, and $\mathrm{C^*_{elvoc}}$ determined the local minimum $GR_{meas,elvoc}$ at the right side of $D_{p,act}$. Therefore, $\mathrm{C^*}$ and $\mathrm{C_\infty}$ were basically determined by the measured *GR* (local maximum and local minimum) and not sensitive to x_0. As shown in Table 1, the condensing organic vapor concentrations $\mathrm{C_{elvoc}}$ were $1.7\times10^7 – 1.7\times10^8$ cm^{-3}. The saturation vapor concentration $\mathrm{C^*_{elvoc}}$ were 3.3×10^6- 5.2×10^7 cm^{-3}. They were within the orders of magnitude of 10^7-10^8 cm^{-3} and 10^6-10^7 cm^{-3} suggested by Kulmala et al. (2004b), respectively.

For comparison, the *GR* calculated from appearance time method was also shown in Figure 9 (blue cross) for > 3 nm particles on May 15, February 18 and February 19, as well as for sub-3 nm particles on May 20 when particle growth was relatively slow. It can be seen that the *GR* on May 20 calculated from the two methods agreed well with each other, lending credit to our GDE method. The GR in >10 nm sizes was usually underestimated by GR_{elvoc}. This could be interpreted as other condensing vapors with higher volatility may contribute to particle growth in the larger particles. It should be noted that the appearance time method followed the time steps when newly-formed particles appeared in successive size bins and thus the GR calculated from appearance time method as not the growth rates at the same instant in time.

For all the 8 nucleation events, Table 1 summarizes the measured values of overall growth rate in 1.4-3 nm ($GR_{1.4\text{-}3}$), maximum growth rate in 1.4-3 nm ($GR_{max,1.4\text{-}3}$), overall growth rate in 3-20 nm ($GR_{3\text{-}20}$), nucleation rate ($J_{1.4}$), activation diameter ($D_{p,act}$), CS, and temperature (T) during the event periods with maximum nucleation rates. Corresponding estimates of Mikkonen H_2SO_4 proxy, $\mathrm{C}_{\mathrm{elvoc}}$, and $\mathrm{C}^{*}_{\mathrm{elvoc}}$ were shown in the right 3 columns. It can be seen that in comparison with more conventional Type A events, Type B events usually occurred with (1) higher $J_{1.4}$, $GR_{max,1.4\text{-}3}$, $GR_{1.4\text{-}3}$, $\mathrm{C}_{\mathrm{elvoc}}$, and CS; (2) smaller $D_{p,act}$; and (3) lower T. However, the H_2SO_4 proxy and $GR_{3\text{-}20}$ were similar in Type A and Type B events. Based on these estimations, we concluded that higher ELVOC concentration $\mathrm{C}_{\mathrm{elvoc}}$ was the key factor leading to the higher $J_{1.4}$ and $GR_{1.4\text{-}3}$, which in turn resulted in the different size spectrum pattern in Type B events ("up-side-down volcano") from in Type A events ("volcano").

It should be noted that the organic vapor concentrations $\mathrm{C}_{\mathrm{elvoc}}$ in this study were not directly measured, but estimated based on Eq. (4-5). $\mathrm{C}_{\mathrm{elvoc}}$, [H_2SO_4], mole fraction x_{D_p} and growth rates calculated using Eq. (4-5) were for an instant in time. Aerosol dynamic processes, such as nucleation, coagulation, and the condensation growth of H_2SO_4 and water vapor, were not considered explicitly in Eq. (4-5). In addition, bulk thermodynamics was applied in Eq. (5) for extremely small clusters/particles of sub-3 nm sizes. Therefore, although our calculation provided a possibility to explain the size dependence of growth rate observed in the polluted urban atmosphere, C_{elvoc} in this study was subject to uncertainties in (1) the growth rate derived from the GDE method, (2) the theory by which the growth rate was related to the organic vapor concentration, and (3) H_2SO_4 level which was calculated using Mikkonen et al. (2011) proxy.

3.5 Inhibited particle growth to CCN-active sizes in strong nucleation events of Type B2

Type B2 was strong nucleation event that produced rather high concentrations of new particles in sub-20 nm size range (Figure 3d). High concentrations of activating vapor in these events (e.g., C_∞: 1.4-2.0 $\times 10^8$ cm^{-3} on February 18 and March 4) should favor a banana-shape NPF event with fast growth of particles >20 nm, due to weakened Kelvin effect. However, it was puzzling to us why new particles accumulated in 2-20 nm and did not grow further on Type B2 event days (see Figure 3d). We first examined the air mass trajectory characteristics of Type B2 events. Compared with Type B1, Type B2 was characterized by long range transport air masses from far north of China and Mongolia. The lumped trajectories with insignificant wind direction change imply that the air mass in Type B2 event was quite uniform. In addition, meteorological and chemical variables (high solar radiation flux and wind speed, low temperature, $PM_{2.5}$, SO_2, NO_2, CO and O_3, green lines in Figure 5) collectively suggested that Type B2 was typical regional event in homogeneous cold air masses. Therefore, the interrupted growth of new particles was not likely to be a result of wind direction change.

As seen from Figure 5, meteorological variables on Type B2 days were generally more favorable in aiding particle growth than on Type B1 days: lower $PM_{2.5}$, lower temperature, and higher solar radiation flux. The unfavorable factors in Type B2 events, however, included lower concentrations of SO_2, NO_2, and CO (anthropogenic emission indicators), lower secondary photochemical product indicators O_3 and lower particle phase sulfate in 100-1000 nm (X. Ge, private communication, 2015, X. Ge conducted simultaneous AMS measurement during our measurement periods). All these evidences suggested that further particle growth in Type B2 events was limited by certain condensing vapor other than ELVOC. Consequently, although there was a pool of sub-20 nm particles, they were not further “activated” due to the low availability of this condensing vapor. Following the terminology of Donahue et al. (2011, 2012), we called this condensing vapor LVOC (low volatility organic compounds)

The above hypothesis was sound if we considered that the identity of LVOC for the growth of particles > 20 nm could be different from ELVOC for sub-3 nm particle growth. Hirsikko et al. (2005) observed that $GR_{3\text{-}20}$ demonstrated an opposite seasonal cycle to $GR_{1.3\text{-}3}$: $GR_{3\text{-}20}$ was higher in summer, whereas $GR_{1.3\text{-}3}$ was higher in winter. This suggested that the condensing vapors were different in identity for particles of different sizes. Hirsikko et al. (2005) attributed the condensing vapors for $GR_{3\text{-}20}$ to biogenetic VOCs. In our urban atmosphere, according to Figure 5, LVOC was more likely to be from anthropogenic sources associated with SO_2, NO_x and CO emissions. A picture of the growth process was thus like this: ELVOC of lower volatility, lower concentration and higher water solubility activated inorganic nuclei and accelerated particle growth in smaller sizes. This in turn assisted in the condensation of LVOC of high volatility, low solubility, but with larger amount of mass. The further growth of particles >20 nm, which means significant increment of particle mass, needed continuous supply of LVOC from the anthropogenic sources. On the Type B2 days, LVOC supply was not adequate (low SO_2, CO and NO_x). As a result, continuous banana-shape particle growth did not take place.

4. Conclusion

NPF can contribute to CCN only after going through nucleation, initial growth steps and subsequent growth to CCN-active sizes. This study provided the evidences of limiting factors in these processes in a polluted urban atmosphere in China. We observed atmospheric nucleation events on 42 out of total 90 observation days, but particles could grow to CCN-active sizes on only 9 days, which was equivalent to 9 conventional NPF events. In summer, strict emission control measures during the 2014 Youth Olympic Games resulted in relatively low $PM_{2.5}$ and anthropogenic trace gases (SO_2, NO_2, CO and O_3) levels. Infrequent nucleation was thus limited by both low concentrations of gaseous precursors and high temperature and RH in summer. In more polluted winter and spring atmosphere, precursor supply was not limiting anymore; nucleation occurred once meteorological conditions were favorable (i.e. low *CS* and temperature/RH, higher solar radiation). However, for the further growth of sub-3 nm particles to CCN-active sizes, anthropogenic gaseous precursors again became limiting factors.

A simplified GDE method was used in this study to calculate particle formation rates first and then growth rates. Nucleation events were strong in the polluted urban atmosphere of Nanjing. Initial $J_{1.4}$ at the onset and peak $J_{1.4}$ at the noontime could be up to 2.1×10^{2} cm^{-3} s^{-1} and 2.5×10^{3} cm^{-3} s^{-1}, respectively, during the 8 nucleation events selected from different seasons. The diurnal variation of

$J_{1.4}$ implied that nucleation was usually linked to sunlight induced photochemistry. Time-dependent $J_{1.4}$ showed good linear correlations with the H_2SO_4 proxy for every single event, except a day with significant nocturnal nucleation. However, the correlation between $J_{1.4}$ and the H_2SO_4 proxy for all 8 events deteriorated, which might reflect the effect of temperature or assisting vapor concentration in the nucleation. The deteriorated correlation could also be due to the lower predictive ability of the H_2SO_4 proxy in the polluted urban atmosphere for different seasons.

In all nucleation events, a local maximum growth rate was observed between 1-3 nm with GR up to 25 nm h^{-1}. This means GR was not monotonically increasing with particle size. The overall $GR_{1.4-3}$, however, was still smaller than GR_{3-20}, if particles could grow beyond 3 nm. The local maximum growth rate was interpreted as the solvation effect of organic activating vapor in newly formed inorganic nuclei. Based on our estimation, high ELVOC concentration of 2.3×10^7 - 2.0×10^8 cm^{-3} was expected to be the key factor leading to high $GR_{1.4-3}$. The varying GR of new particle in turn resulted in the different particle growth patterns that we observed in Nanjing.

Our results call for a more robust proxy of gaseous H2SO4 to be developed for polluted urban conditions. The study also highlighted the importance of estimating or measuring activating organic vapor levels (using CI-APi-TOF, for example) in the initial growth steps of atmospheric NPF. Our year-round measurement data provided valuable size evolution data of sub-3 nm clusters/particles to evaluate previous aerosol dynamic models of new particle formation. A robust dynamic model was needed to appropriately treat all aerosol and gas-phase processes in the initial growth steps.

Acknowledgements

This work was supported by National Science Foundation of China (41405116, 41275142, 41575122), Natural Science Foundation of Jiangsu Province (BK20140989), and Jiangsu Specially Appointed Professor grant. The measurement campaigns were partially funded by the Priority Academic Program Development of Jiangsu Higher Education Institutions (PAPD). We thank Dr. Vijay P. Kanawade and Dr. Xinlei Ge for valuable discussion.

References:

Almeida, J., Schobesberger, S., Kurten, A., Ortega, I. K., Kupiainen-Maatta, O., Praplan, A. P., Adamov, A., Amorim, A., Bianchi, F., Breitenlechner, M., David, A., Dommen, J., Donahue, N. M., Downard, A., Dunne, E., Duplissy, J., Ehrhart, S., Flagan, R. C., Franchin, A., Guida, R., Hakala, J., Hansel, A., Heinritzi, M., Henschel, H., Jokinen, T., Junninen, H., Kajos, M., Kangasluoma, J., Keskinen, H., Kupc, A., Kurten, T., Kvashin, A. N., Laaksonen, A., Lehtipalo, K., Leiminger, M., Leppa, J., Loukonen, V., Makhmutov, V., Mathot, S., McGrath, M. J., Nieminen, T., Olenius, T., Onnela, A., Petaja, T., Riccobono, F., Riipinen, I., Rissanen, M., Rondo, L., Ruuskanen, T., Santos, F. D., Sarnela, N., Schallhart, S., Schnitzhofer, R., Seinfeld, J. H., Simon, M., Sipila, M., Stozhkov, Y., Stratmann, F., Tome, A., Trostl, J., Tsagkogeorgas, G., Vaattovaara, P., Viisanen, Y., Virtanen, A., Vrtala, A., Wagner, P. E., Weingartner, E., Wex, H., Williamson, C., Wimmer, D., Ye, P., Yli-Juuti, T., Carslaw, K. S., Kulmala, M., Curtius, J., Baltensperger, U., Worsnop, D. R., Vehkamaki, H., and Kirkby, J.: Molecular understanding of sulphuric acid-amine particle nucleation in the atmosphere, Nature, 502(7471), 359-363, doi:10.1038/nature12663, 2013.

Anttila, T., Kerminen, V. M., Kulmala, M., Laaksonen, A., and O'Dowd, C. D.: Modelling the formation of organic particles in the atmosphere, Atmos. Chem. Phys., 4(4), 1071-1083, doi: 10.5194/acp-4-1071-2004, 2004.

Asmi, E., Sipilä, M., Manninen, H. E., Vanhanen, J., Lehtipalo, K., Gagné, S., Neitola, K., Mirme, A., Mirme, S., Tamm, E., Uin, J., Komsaare, K., Attoui, M., and Kulmala, M.: Results of the first air ion spectrometer calibration and intercomparison workshop, Atmos. Chem. Phys., 9(1), 141-154, doi: 10.5194/acp-9-141-2009, 2009.

Brus, D., Neitola, K., Hyvärinen, A.-P., Petäjä, T., Vanhanen, J., Sipilä, M., Paasonen, P., Kulmala, M., and Lihavainen, H.: Homogenous nucleation of sulfuric acid and water at close to atmospherically relevant conditions, Atmos. Chem. Phys., 11(11), 5277-5287, doi: 10.5194/acp-11-5277-2011, 2011.

Chan, C. K., and Yao, X.: Air pollution in mega cities in China, Atmos. Environ., 42(1), 1-42, doi: :10.1016/j.atmosenv.2007.09.003.

Donahue, N. M., Trump, E. R., Pierce, J. R., and Riipinen, I.: Theoretical constraints on pure vapor-pressure driven condensation of organics to ultrafine particles, Geophys. Res. Lett., 38(16), L16801, doi: 10.1029/2011gl048115, 2011.

Donahue, N. M., Kroll, J. H., Pandis, S. N., and Robinson, A. L.: A two-dimensional volatility basis set – Part 2: Diagnostics of organic-aerosol evolution, Atmos. Chem. Phys., 12(2), 615-634, doi: 10.5194/acp-12-615-2012, 2012.

Ehn, M., Thornton, J. A., Kleist, E., Sipila, M., Junninen, H., Pullinen, I., Springer, M., Rubach, F., Tillmann, R., Lee, B., Lopez-Hilfiker, F., Andres, S., Acir, I.-H., Rissanen, M., Jokinen, T., Schobesberger, S., Kangasluoma, J., Kontkanen, J., Nieminen, T., Kurten, T., Nielsen, L. B., Jorgensen, S., Kjaergaard, H. G., Canagaratna, M., Maso, M. D., Berndt, T., Petaja, T., Wahner, A., Kerminen, V. M., Kulmala, M., Worsnop, D. R., Wildt, J., and Mentel, T. F.: A large source of low-volatility secondary organic aerosol, Nature, 506(7489), 476-479, doi: 10.1038/nature13032, 2014.

Herrmann, E., Ding, A. J., Kerminen, V.-M., Petäjä, T., Yang, X. Q., Sun, J. N., Qi, X. M., Manninen, H., Hakala, J., Nieminen, T., Aalto, P. P., Kulmala, M., and Fu, C. B.:: Aerosols and nucleation in eastern China: first insights from the new SORPES-NJU station, Atmos. Chem. Phys., 14, 2169-2183, doi: 10.5194/acp-14-2169-2014, 2014.

Hirsikko, A., Laakso, L., Horrak, U., Aalto, P. P., Kerminen, V. M., and Kulmala, M.: Annual and size dependent variation of growth rates and ion concentrations in boreal forest, Boreal Environ. Res., 10, 357-469, 2005.

Jiang, J., Chen, M., Kuang, C., Attoui, M., and McMurry, P. H.: Electrical Mobility Spectrometer Using a Diethylene Glycol Condensation Particle Counter for Measurement of Aerosol Size

Distributions Down to 1 nm, Aerosol Sci. Technol., 45(4), 510-521, doi: 10.1080/02786826.2010.547538, 2011a.

Jiang, J., Zhao, J., Chen, M., Eisele, F. L., Scheckman, J., Williams, B. J., Kuang, C., and McMurry, P. H.: First Measurements of Neutral Atmospheric Cluster and 1-2 nm Particle Number Size Distributions During Nucleation Events, Aerosol Sci. Technol., 45(4), II-V, doi: 10.1080/02786826.2010.546817, 2011b.

Jokinen, T., Sipilä, M., Junninen, H., Ehn, M., Lönn, G., Hakala, J., Petäjä, T., Mauldin III, R. L., Kulmala, M., and Worsnop, D. R.: Atmospheric sulphuric acid and neutral cluster measurements using CI-APi-TOF, Atmos. Chem. Phys., 12(9), 4117-4125, doi: 10.5194/acp-12-4117-2012, 2012.

Junninen, H., Hulkkonen, M., Riipinen, I., Nieminen, T., Hirsikko, A., Suni, T., Boy, M., Lee, S.-H., Vana, M., Tammet, T., Kerminen, V. M., and Kulmala, M.: Observations on nocturnal growth of atmospheric clusters, Tellus Ser. B, 60, 365-371, doi:10.1111/j.1600-0889.2008.00356.x, 2008.

Junninen, H., Ehn, M., Petäjä, T., Luosujärvi, L., Kotiaho, T., Kostiainen, R., Rohner, U., Gonin, M., Fuhrer, K., Kulmala, M., and Worsnop, D. R.: A high-resolution mass spectrometer to measure atmospheric ion composition, Atmos. Meas. Tech., 3, 1039-1053, doi: 10.5194/amtd-3-599-2010, 2010.

Kangasluoma, J., Kuang, C., Wimmer, D., Rissanen, M. P., Lehtipalo, K., Ehn, M., Worsnop, D.R., Wang, J., Kulmala, M. and Petäjä, T.: Sub-3 nm particle size and composition dependent response of a nano-CPC battery. Atmos. Meas. Tech., 7, 689-700, doi: 10.5194/amt-7-689-2014, 2014.

Kirkby, J., Curtius, J., Almeida, J., Dunne, E., Duplissy, J., Ehrhart, S., Franchin, A., Gagne, S., Ickes, L., Kurten, A., Kupc, A., Metzger, A., Riccobono, F., Rondo, L., Schobesberger, S., Tsagkogeorgas, G., Wimmer, D., Amorim, A., Bianchi, F., Breitenlechner, M., David, A., Dommen, J., Downard, A., Ehn, M., Flagan, R. C., Haider, S., Hansel, A., Hauser, D., Jud, W., Junninen, H., Kreissl, F., Kvashin, A., Laaksonen, A., Lehtipalo, K., Lima, J., Lovejoy, E. R., Makhmutov, V., Mathot, S., Mikkila, J., Minginette, P., Mogo, S., Nieminen, T., Onnela, A., Pereira, P., Petaja, T., Schnitzhofer, R., Seinfeld, J. H., Sipila, M., Stozhkov, Y., Stratmann, F., Tome, A., Vanhanen, J., Viisanen, Y., Vrtala, A., Wagner, P. E., Walther, H., Weingartner, E., Wex, H., Winkler, P. M., Carslaw, K. S., Worsnop, D. R., Baltensperger, U., and Kulmala, M.: Role of sulphuric acid, ammonia and galactic cosmic rays in atmospheric aerosol nucleation, Nature, 476(7361), 429-433, doi:10.1038/nature10343, 2011.

Kuang, C., Chen, M., Zhao, J., Smith, J., McMurry, P. H., and Wang, J.: Size- and time-resolvedt growth rate measurements of 1 to 5 nm freshly formed atmospheric nuclei, Atmos. Chem. Phys., 12(9), 3573-3589, doi: 10.5194/acpd-11-25427-2011, 2012.

Kulmala, M., Pirjola, L., and Makela, J. M.: Stable sulfate clusters as a source of new atmospheric particles, Nature, 404, 60-66, doi: 10.1038/35003550, 2000.

Kulmala, M., Laakso, L., Lehtinen, K. E. J., Riipinen, I., Dal Maso, M., Lauria, A., Kerminen, V. M., Birmili, W., McMurry, P.H.: Formation and growth rates of ultrafine atmosphere particles: A review of observations, J. Aerosol. Sci., 35, 143-176, 2004a.

Kulmala, M., Kerminen, V. M., Anntila, T., Laaksonen, A., and O'Dowd, C. D.: Organic aerosol formation via sulfate cluster activation, J. Geophys. Res., 109, D04205, doi: 10.1029/2003JD003961, 2004b.

Kulmala, M., Laakso, L., Lehtinen, K. E. J., Riipinen, I., Dal Maso, M., Anttila, T., Kerminen, V.-M., Hõrrak, U., Vana, M., and Tammet, H.: Initial steps of aerosol growth, Atmos. Chem. Phys., 4(11), 2553-2560, doi: 10.5194/acp-4-2553-2004, 2004c.

Kulmala, M., Petäjä, T., Nieminen, T., Sipilä, M., Manninen, H. E., Lehtipalo, K., Dal Maso, M., Aalto, P. P., Junninen, H., Paasonen, P., Riipinen, I., Lehtinen, K. E. J., Laaksonen, A., and Kerminen, V. M.: Measurement of the nucleation of atmospheric aerosol particles, Nat. Protocols, 7(9), 1651-1667, doi: 10.1038/nprot.2012.091, 2012.

Kulmala, M., Kontkanen, J., Junninen, H., Lehtipalo, K., Manninen, H. E., Nieminen, T., Petäjä, T., Sipilä, M., Schobesberger, S., Rantala, P., Franchin, A., Jokinen, T., Järvinen, E., Äijälä, M., Kangasluoma, J., Hakala, J., Aalto, P. P., Paasonen, P., Mikkilä, J., Vanhanen, J., Aalto, J., Hakola, H., Makkonen, U., Ruuskanen, T., Mauldin, R. L., Duplissy, J., Vehkamäki, H., Bäck, J., Kortelainen, A., Riipinen, I., Kurtén, T., Johnston, M. V., Smith, J. N., Ehn, M., Mentel, T. F., Lehtinen, K. E. J., Laaksonen, A., Kerminen, V. M., and Worsnop, D. R.: Direct Observations of

Atmospheric Aerosol Nucleation, Science, 339(6122), 943-946, doi: 10.1126/science.1227385, 2013.

Kulmala, M., Petäjä, T., Ehn, M., Thornton, J., Sipilä, M., Worsnop, D. R. and Kerminen, V. M.: Chemistry of Atmospheric Nucleation: On the Recent Advances on Precursor Characterization and Atmospheric Cluster Composition in Connection with Atmospheric New Particle Formation, Annu. Rev. Phys. Chem., 65, 21–37, doi: 10.1146/annurev-physchem-040412-110014, 2014.

Kürten, A., Jokinen, T., Simon, M., Sipilä, M., Sarnela, N., Junninen, H., Adamov, A., Almeida, J., Amorim, A., Bianchi, F., Breitenlechner, M., Dommen, J., Donahue, N. M., Duplissy, J., Ehrhart, S., Flagan, R. C., Franchin, A., Hakala, J., Hansel, A., Heinritzi, M., Hutterli, M., Kangasluoma, J., Kirkby, J., Laaksonen, A., Lehtipalo, K., Leiminger, M., Makhmutov, V., Mathot, S., Onnela, A., Petäjä, T., Praplan, A. P., Riccobono, F., Rissanen, M. P., Rondo, L., Schobesberger, S., Seinfeld, J. H., Steiner, G., Tomé, A., Tröstl, J., Winkler, P. M., Williamson, C., Wimmer, D., Ye, P., Baltensperger, U., Carslaw, K. S., Kulmala, M., Worsnop, D. R., and Curtius, J.: Neutral molecular cluster formation of sulfuric acid–dimethylamine observed in real time under atmospheric conditions, Proc. Natl. Acad. Sci. U.S.A., 111(42), 15019-15024, doi:10.1073/pnas.1404853111, 2014.

Lee, S. H., Young, L. H., Benson, D. R., Kulmala, M., Junninen, H., Suni, T., Campos, T., Rogers, D. C., and Jensen, J.: Observations of nighttime new particle formation in the troposphere, J. Geophys. Res., 113, D10210, doi: 10210.11029/12007JD009351, 2008.

Lehtipalo, K., Sipilä, M., Riipinen, I., Nieminen, T., and Kulmala, M.: Analysis of atmospheric neutral and charged molecular clusters in boreal forest using pulse-height CPC, Atmos. Chem. Phys., 9, 4177–4184, 2009.

Lehtipalo, K., Sipila, M., Junninen, H., Ehn, M., Berndt, T., Kajos, M. K., Worsnop, D. R., Petaja, T., and Kulmala, M.: Nanoparticles in boreal forest and coastal environment: a comparison of observations and implications of the nucleation mechanism, Atmos. Chem. Phys., 10, 7009-7016, 2010.

Lehtipalo, K., Sipila, M., Junninen, H., Ehn, M., Berndt, T., Kajos, M. K., Worsnop, D. R., Petaja, T., and Kulmala, M.: Observations of Nano-CN in the Nocturnal Boreal Forest, Aerosol Sci. Technol., 45(4), 499-509, doi: 10.1080/02786826.2010.547537, 2011.

Lehtipalo., K., Leppä, J., Kontkanen., J., Kangasluoma., J., Franchin., A., Wimmer., D., Schobesberger., S., Junninen., H., Petäjä, T., Sipilä, M., Mikkilä, J., Vanhanen., J., Worsnop., D. R., and Kulmala, M.: Methods for determining particle size distribution and growth rates between 1 and 3 nm using the Particle Size Magnifier, Boreal Environ. Res., 19, 215–236, 2014.

Matsui, H., Koike, M., Takegawa, N., Kondo, Y., Takami, A., Takamura, T., Yoon, S., Kim, S. W., Lim, H. C., and Fast, J. D.: Spatial and temporal variations of new particle formation in East Asia using an NPF-explicit WRF-chem model: North-south contrast in new particle formation frequency, J. Geophys. Res., 118(20), 11,647-611,663, doi:10.1002/jgrd.50821, 2013.

Merikanto, J., Spracklen, D. V., Mann, G. W., Pickering, S. J., and Carslaw, K. S.: Impact of nucleation on global CCN, Atmos. Chem. Phys., doi: 10.5194/acp-9-8601-2009, 9, 8601-8616, 2009.

Mikkonen, S., Romakkaniemi, S., Smith, J. N., Korhonen, H., Petäjä, T., Plass-Duelmer, C., Boy, M., McMurry, P. H., Lehtinen, K. E. J., Joutsensaari, J., Hamed, A., Mauldin III, R. L., Birmili, W., Spindler, G., Arnold, F., Kulmala, M., and Laaksonen, A.: A statistical proxy for sulphuric acid concentration, Atmos. Chem. Phys., 11:11319-11334, doi: 10.5194/acpd-11-20141-2011, 2011.

Nieminen, T., Lehtinen, K. E. J., and Kulmala, M.: Sub-10 nm particle growth by vapor condensation - effects of vapor molecule size and particle thermal speed, Atmos. Chem. Phys., 10(20), 9773-9779, doi: 10.5194/acp-10-9773-2010, 2010.

Ortega, I. K., Suni, T., Gronholm, T., Boy, M., Hakola, H., Hellen, H., Valmari, T., Arvela, H., Vehkamaki, H., and Kulmala, M.: Is eucalyptol the cause of nocturnal events observed in Australia?, Boreal Environ. Res., 14(4), 606-615, 2009.

Ortega, I. K., Suni, T., Boy, M., Grönholm, T., Manninen, H. E., Nieminen, T., Ehn, M., Junninen, H., Hakola, H., Hellén, H., Valmari, T., Arvela, H., Zegelin, S., Hughes, D., Kitchen, M., Cleugh, H., Worsnop, D. R., Kulmala, M., and Kerminen, V. M.: New insights into nocturnal nucleation, Atmos. Chem. Phys., 12(9), 4297-4312, doi:10.5194/acp-12-4297-2012, 2012.

Petäjä, T., Mauldin, III, R. L., Kosciuch, E., McGrath, J., Nieminen, T., Paasonen, P., Boy, M., Adamov, A., Kotiaho, T., and Kulmala, M.: Sulfuric acid and OH concentrations in a boreal forest site, Atmos. Chem. Phys., 9, 7435–7448, doi:10.5194/acp-9-7435-2009, 2009.

Pierce, J. R., and Adams, P. J.: Uncertainty in global CCN concentrations from uncertain aerosol nucleation and primary emission rates, Atmos. Chem. Phys., 9(4), 1339-1356, doi: 10.5194/acp-9-1339-2009, 2009.

Riccobono, F., Schobesberger, S., Scott, C. E., Dommen, J., Ortega, I. K., Rondo, L., Almeida, J., Amorim, A., Bianchi, F., Breitenlechner, M., David, A., Downard, A., Dunne, E. M., Duplissy, J., Ehrhart, S., Flagan, R. C., Franchin, A., Hansel, A., Junninen, H., Kajos, M., Keskinen, H., Kupc, A., Kürten, A., Kvashin, A. N., Laaksonen, A., Lehtipalo, K., Makhmutov, V., Mathot, S., Nieminen, T., Onnela, A., Petäjä, T., Praplan, A. P., Santos, F. D., Schallhart, S., Seinfeld, J. H., Sipilä, M., Spracklen, D. V., Stozhkov, Y., Stratmann, F., Tomé, A., Tsagkogeorgas, G., Vaattovaara, P., Viisanen, Y., Vrtala, A., Wagner, P. E., Weingartner, E., Wex, H., Wimmer, D., Carslaw, K. S., Curtius, J., Donahue, N. M., Kirkby, J., Kulmala, M., Worsnop, D. R., and Baltensperger, U.: Oxidation Products of Biogenic Emissions Contribute to Nucleation of Atmospheric Particles, Science, 344(6185), 717-721, doi:10.1126/science.1243527, 2014.

Riipinen, I., Yli-Juuti, T., Pierce, J. R., Petaja, T., Worsnop, D. R., Kulmala, M., and Donahue, N. M.: The contribution of organics to atmospheric nanoparticle growth, Nature Geosci., 5(7), 453-458, doi: 10.1038/NGEO1499, 2012.

Russell, L. M., Mensah, A. A., Fischer, E. V., Sive, B. C., Varner, R. K., Keene, W. C., Stutz, J., and Pszenny, A. A. P.: Nanoparticle growth following photochemical α- and β-pinene oxidation at Appledore Island during International Consortium for Research on Transport and Transformation/Chemistry of Halogens at the Isles of Shoals 2004, J. Geophys. Res., 112(D10), D10S21, doi:10.1029/2006jd007736, 2007.Seinfeld, J. H., and Pandis, S. N.: Atmospheric chemistry and physics: from air pollution to climate change, 2nd ed., John Wiley and Sons. Inc., New York, 2006.

Schobesberger, S., Junninen, H., Bianchi, F., Lönn, G., Ehn, M., Lehtipalo, K., Dommen, J., Ehrhart, S., Ortega, I. K., Franchin, A., Nieminen, T., Riccobono, F., Hutterli, M., Duplissy, J., Almeida, J., Amorim, A., Breitenlechner, M., Downard, A. J., Dunne, E. M., Flagan, R. C., Kajos, M., Keskinen, H., Kirkby, J., Kupc, A., Kürten, A., Kurtén, T., Laaksonen, A., Mathot, S., Onnela, A., Praplan, A. P., Rondo, L., Santos, F. D., Schallhart, S., Schnitzhofer, R., Sipilä, M., Tomé, A., Tsagkogeorgas, G., Vehkamäki, H., Wimmer, D., Baltensperger, U., Carslaw, K. S., Curtius, J., Hansel, A., Petäjä, T., Kulmala, M., Donahue, N. M., and Worsnop, D. R.: Molecular understanding of atmospheric particle formation from sulfuric acid and large oxidized organic molecules, Proc. Natl. Acad. Sci. U.S.A., doi:10.1073/pnas.1306973110, 2013.

Sipila, M., Lehtipalo, K., Attoui, M., Neitola, K., Petäjä, T., Aalto, P. P., O'Dowd, C. D., and Kulmala, M.: Laboratory Verification of PH-CPC's Ability to Monitor Atmospheric Sub-3 nm Clusters, Aerosol Sci. Technol., 43(2), 126-135, doi: 10.1080/02786820802506227, 2009.

Spracklen, D. V., Carslaw, K. S., Kulmala, M., Kerminen, V.-M., Sihto, S.-L., Riipinen, I., Merikanto, J., Mann, G. W., Chipperfield, M. P., Wiedensohler, A., Birmili, W., and Lihavainen, H.: Contribution of particle formation to global cloud condensation nuclei concentrations, Geophys. Res. Lett., 35(6), L06808, doi:10.1029/2007GL033038, 2008.

Suni, T., Kulmala, M., Hirsikko, A., Bergman, T., Laakso, L., Aalto, P. P., Leuning, R., Cleugh, H., Zegelin, S., Hughes, D., van Gorsel, E., Kitchen, M., Vana, M., Hõrrak, U., Mirme, S., Mirme, A., Sevanto, S., Twining, J., and Tadros, C.: Formation and characteristics of ions and charged aerosol particles in a native Australian Eucalypt forest, Atmos. Chem. Phys., 8(1), 129-139, doi:10.5194/acp-8-129-2008, 2008.

Svenningsson, B., Arneth, A., Hayward, S., Holst, T., Massling, A., Swietlicko, E., Hirsikko, A., Junninen, H., Riipinen, I., Vana, M., Dal Maso, M., Hussein, T., and Kulmala, M.: Aerosol particle formation events and analysis of high growth rates observed above a subarctic wetland-forest mosaic, Tellus, 60(B), 353-365, doi:10.1111/j.1600-0889.2008.00351.x, 2008.

Vanhanen, J., Mikkila, J., Lehtipalo, K., Sipila, M., Manninen, H. E., Siivola, E., Petaja, T., and Kulmala, M.: Particle Size Magnifier for Nano-CN Detection, Aerosol Sci. Technol., 45(4), 533-542, doi: 10.1080/02786826.2010.547889, 2011.

von der Weiden, S. L., Drewnick, F., and Borrmann, S.: Particle Loss Calculator – a new software tool for the assessment of the performance of aerosol inlet systems, Atmos. Meas. Tech., 2(2), 479-494, doi: 10.5194/amt-2-479-2009, 2009.

Wiedensohler, A., Cheng, Y. F., Nowak, A., Wehner, B., Achtert, P., Berghof, M., Birmili, W., Wu, Z. J., Hu, M., Zhu, T., Takegawa, N., Kita, K., Kondo, Y., Lou, S. R., Hofzumahaus, A., Holland, F., Wahner, A., Gunthe, S. S., Rose, D., Su, H., and Pöschl, U.: Rapid aerosol particle growth and increase of cloud condensation nucleus activity by secondary aerosol formation and condensation: A case study for regional air pollution in northeastern China, J. Geophys. Res., 114(D2), D00G08, doi:10.1029/2008jd010884, 2009.

Wang, J., and Wexler, A. S.: Adsorption of organic molecules may explain growth of newly nucleated clusters and new particle formation, Geophys. Res. Lett., 11, 2834-2838, doi: 10.1002/grl.50455, 2013.

Wang, J., McGraw, R. L., and Kuang, C.: Growth of atmospheric nano-particles by heterogeneous nucleation of organic vapor, Atmos. Chem. Phys., 13(13), 6523-6531, doi: 10.5194/acp-13-6523-2013, 2013.

Xiao, S., Wang, M. Y., Yao, L., Kulmala, M., Zhou, B., Yang, X., Chen, J. M., Wang, D. F., Fu, Q. Y., Worsnop, D. R., and Wang, L.: Strong atmospheric new particle formation in winter in urban Shanghai, China, Atmos. Chem. Phys., 15(4), 1769-1781, doi: 10.5194/acp-15-1769-2015, 2015.

Yu, H., Gannet Hallar, A., You, Y., Sedlacek, A., Springston, S., Kanawade, V. P., Lee, Y. N., Wang, J., Kuang, C., McGraw, R. L., McCubbin, I., Mikkila, J., and Lee, S. H.: Sub-3 nm particles observed at the coastal and continental sites in the United States, J. Geophys. Res., 119(2), 2013JD020841, doi: 10.1002/2013jd020841, 2014a.

Yu, H., Ortega, J., Smith, J. N., Guenther, A. B., Kanawade, V. P., You, Y., Liu, Y., Hosman, K., Karl, T., Seco, R., Geron, C., Pallardy, S. G., Gu, L., Mikkilä, J., and Lee, S. H.: New Particle Formation and Growth in an Isoprene-Dominated Ozark Forest: From Sub-5 nm to CCN-Active Sizes, Aerosol Sci. Technol., 48(12), 1285-1298, doi: 10.1080/02786826.2014.984801, 2014b.

Yu, F., and Luo, G.: Simulation of particle size distribution with a global aerosol model: contribution of nucleation to aerosol and CCN number concentrations, Atmos. Chem. Phys., 9(20), 7691-7710, doi:10.5194/acp-9-7691-2009, 2009.

Yue, D. L., Hu, M., Zhang, R. Y., Wu, Z. J., Su, H., Wang, Z. B., Peng, J. F., He, L. Y., Huang, X. F., Gong, Y. G., and Wiedensohler, A.: Potential contribution of new particle formation to cloud condensation nuclei in Beijing, Atmos. Environ., 45(33), 6070-6077, doi:10.1016/j.atmosenv.2011.07.037, 2011.

Zhang, K. M., and Wexler, A. S.: A hypothesis for growth of fresh atmospheric nuclei, J. Geophys. Res., 107, 4577, doi: 10.1029/2002JD002180, 2002.

Zhao, J., Eisele, F. L., Titcombe, M., Kuang, C., and McMurry, P. H.: Chemical ionization mass spectrometric measurements of atmospheric neutral clusters using the cluster-CIMS, J. Geophys. Res., 115, D08205, doi: 10.1029/2009JD012606, 2010.

Table 1. Activation diameter ($D_{p,act}$), maximum growth rate in 1.4-3 nm ($GR_{max, 1.4\text{-}3}$), overall growth rate in 1.4-3 nm ($GR_{1.4\text{-}3}$), overall growth rate in 3-20 nm ($GR_{3\text{-}20}$), nucleation rate ($J_{1.4}$), condensation sink (CS), and temperature (T) of selected nucleation events. Estimated gas-phase condensing vapor concentrations $\mathrm{C_{elvoc}}$, pure saturation concentration of condensing vapor over flat surface $\mathrm{C^{*}_{elvoc}}$, and Mikkonen H_2SO_4 proxy were shown in right 3 columns. All data were for the time periods with maximum nucleation rates.

Type	Date	$D_{p,act}$ (nm)	$GR_{max,1.4\text{-}3}$ (nm h^{-1})	$GR_{1.4\text{-}3}$ (nm h^{-1})	$GR_{3\text{-}20}$ (nm h^{-1})	$J_{1.4}$ (cm^{-3}s^{-1})	T (^{o}C)	CS (10^{-2}s^{-1})	Mikkonen H_2SO_4 proxy (cm^{-3})	$\mathrm{C_{elvoc}}$ (cm^{-3})	$\mathrm{C^{*}_{elvoc}}$ (cm^{-3})
A1	May 15, 2014	2.4	6.4	3.6	7.7	3.0×10^{2}	20.8	1.6	2.9×10^{7}	3.5×10^{7}	6.3×10^{6}
A1	Aug 15, 2014	2.4	14.5	7.1	7.7	2.0×10^{2}	26.1	1.8	3.1×10^{7}	8.5×10^{7}	2.1×10^{7}
A2	May 16, 2014	2.4	3.8	1.9	0	95	25.3	1.9	1.4×10^{7}	2.5×10^{7}	4.6×10^{6}
A2	May 20, 2014	2.2	2.9	1.6	0	92	24.1	1.9	1.3×10^{7}	1.7×10^{7}	3.3×10^{6}
B1	Feb 18, 2015	1.6	25.9	4.4	6.0	1.1×10^{3}	8.2	3.3	3.9×10^{7}	1.4×10^{8}	3.0×10^{7}
B1	Dec 27, 2014	1.6	17.7	4.2	5.5	1.9×10^{2}	7.6	2.8	3.5×10^{7}	1.1×10^{8}	2.2×10^{7}
B2	Feb 19, 2015	1.9	25.0	8.9	10.1	8.0×10^{2}	7.4	3.2	3.7×10^{7}	1.7×10^{8}	5.2×10^{7}
B2	Mar 4, 2015	1.9	18.0	5.8	8.7	2.5×10^{3}	3.9	2.2	4.8×10^{7}	1.3×10^{8}	1.1×10^{7}

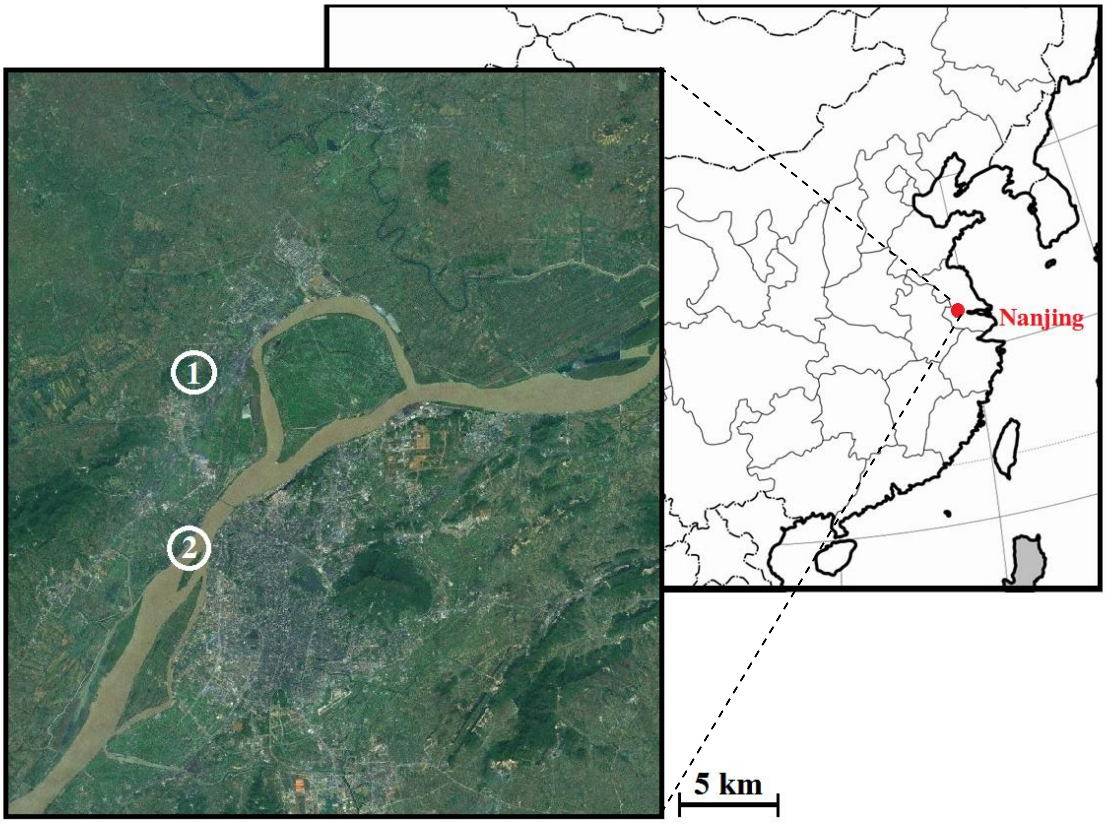

Figure 1. Locations of two urban measurement sites in Nanjing, the second largest megacity in the Yangtze River Delta region, China. ① is the NUIST site and ② is the summer measurement site.

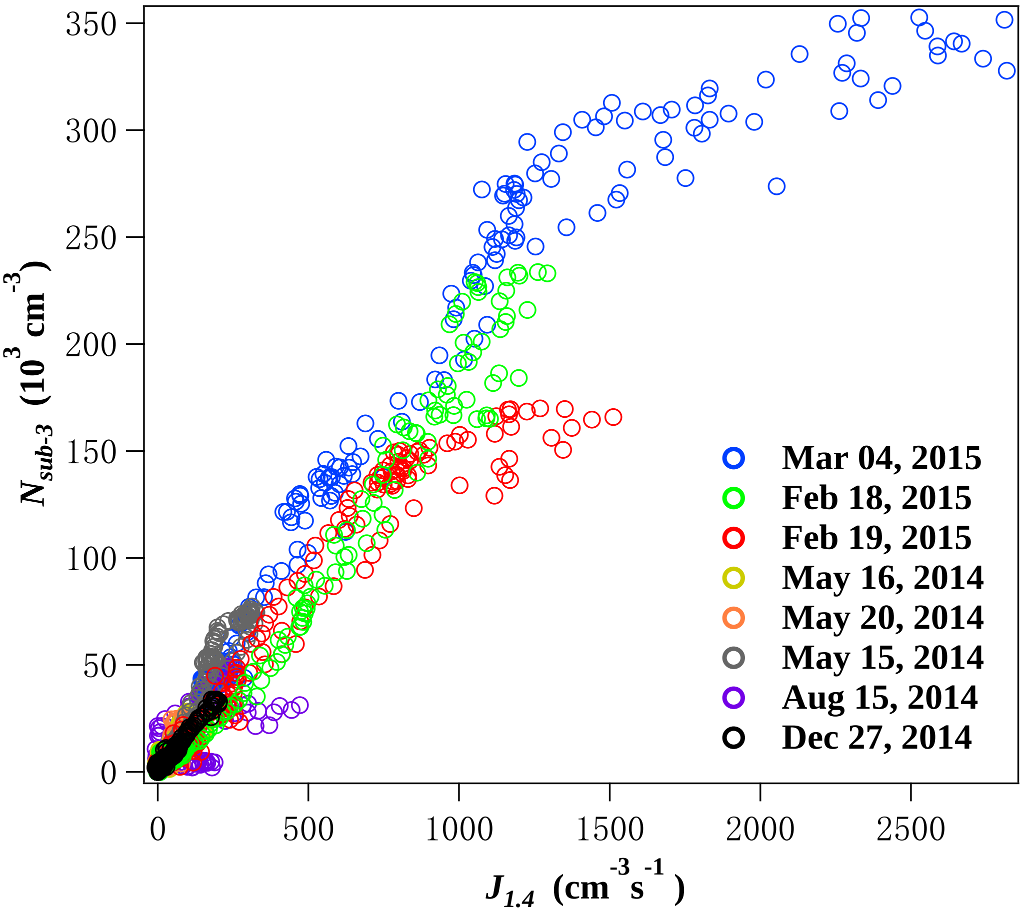

Figure 2. N_{sub-3} *vs.* $J_{1.4}$ in the 8 nucleation events in February, May, December and August during 2014-2015. The events were indicated by different colors (blue: March 1, 2015; green: February 18, 2015; red: February 19, 2015; purple: August 15, 2014; black: December 27, 2014; grey: May 15, 2014; orange: May 20, 2014; yellow: May 16, 2014)

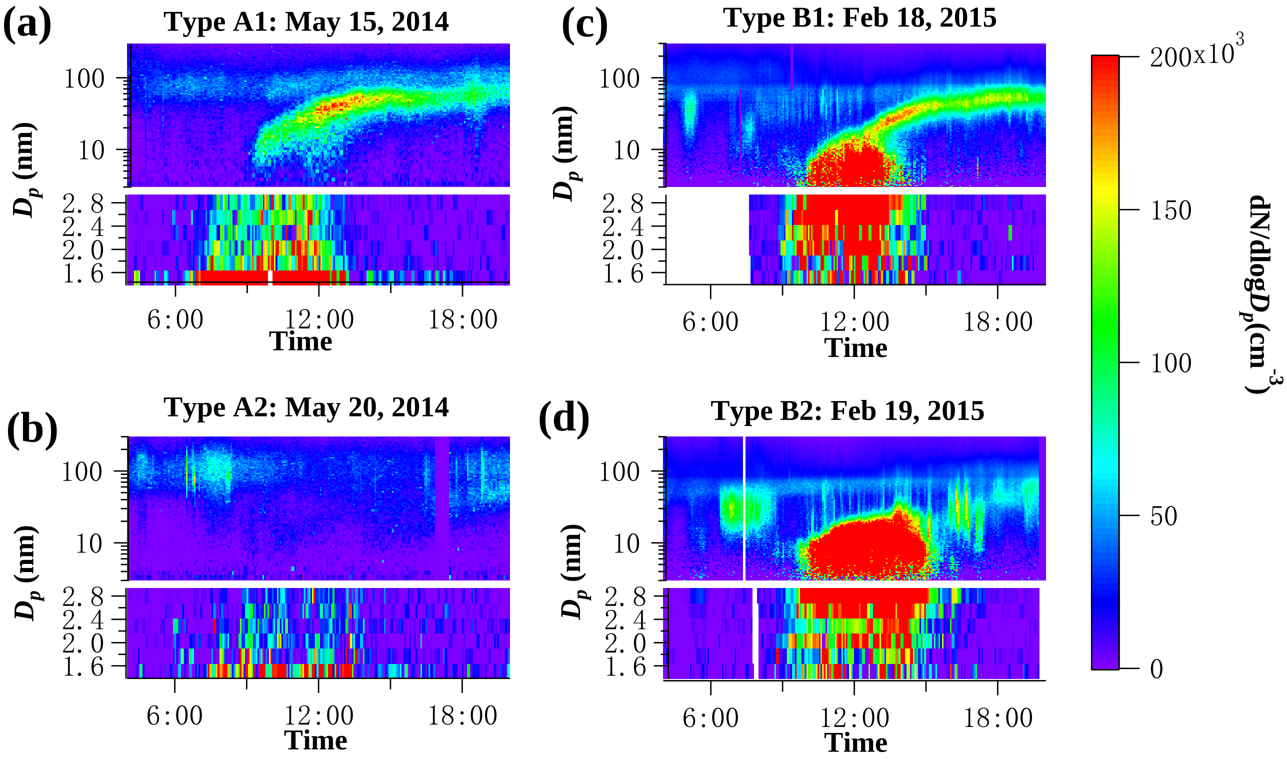

Figure 3. Size spectra of typical (a) Type A1 event on May 15, 2014; (b) Type A2 event on May 20, 2014; (3) Type B1 event on February 18, 2015 and (d) Type B2 event on February 19, 2015 during our measurement period. Size spectra from 3-300 nm (logarithmic scale) and 1.4-3 nm (linear scale) were obtained using SMPS and nCNC, respectively.

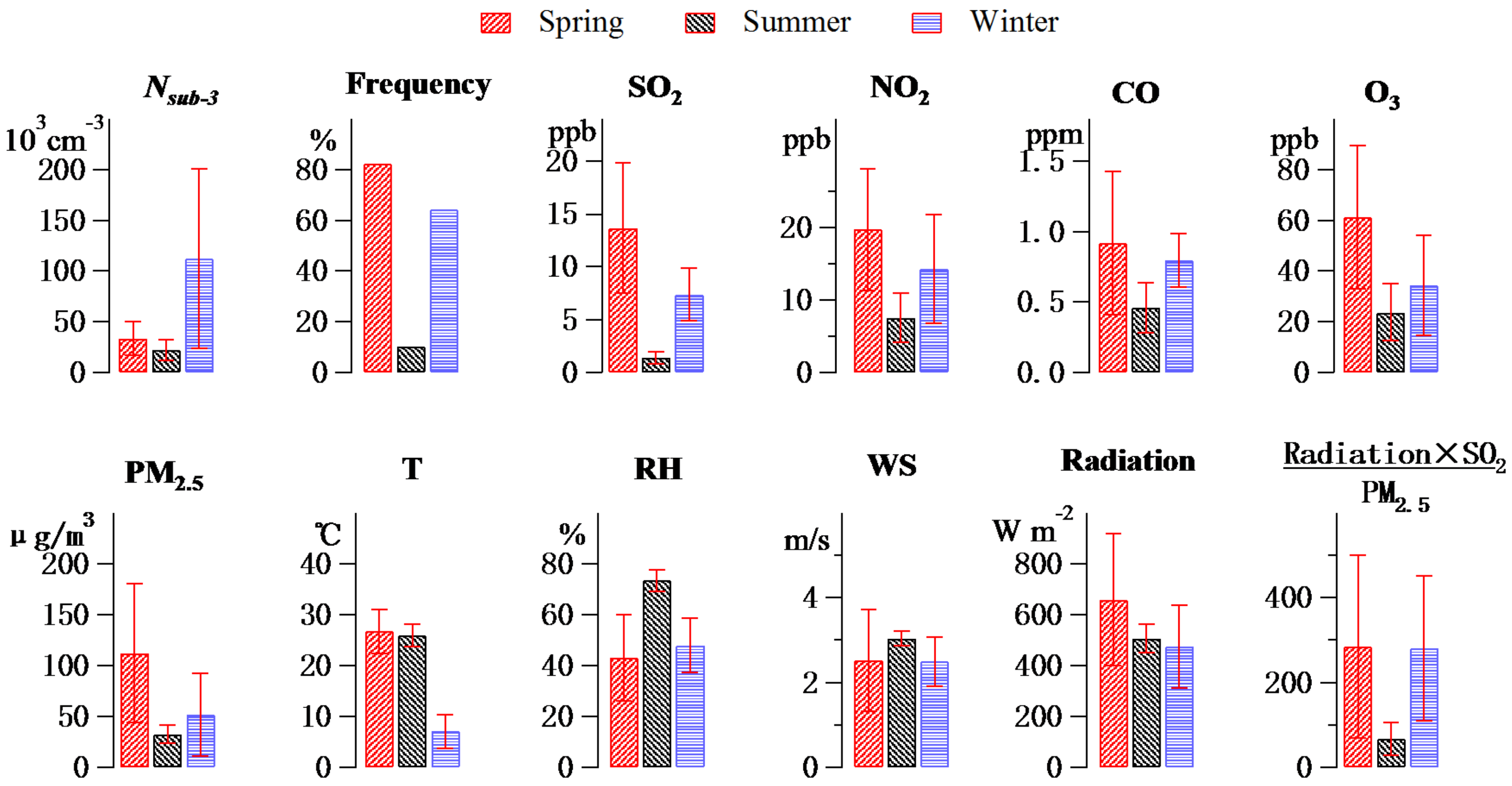

Figure 4. Mean and standard deviation of event-averaged N_{sub-3}, anthropogenic trace gases (SO_2, NO_2, CO and O_3), $PM_{2.5}$, and meteorological variables (temperature, RH, wind speed (WS), solar radiation, and radiation ×$SO_2/PM_{2.5}$) for nucleation events in spring (n=17), summer (n=3) and winter (n=14). Nucleation frequency (the percentage of event days out of total measurement days) was also shown.

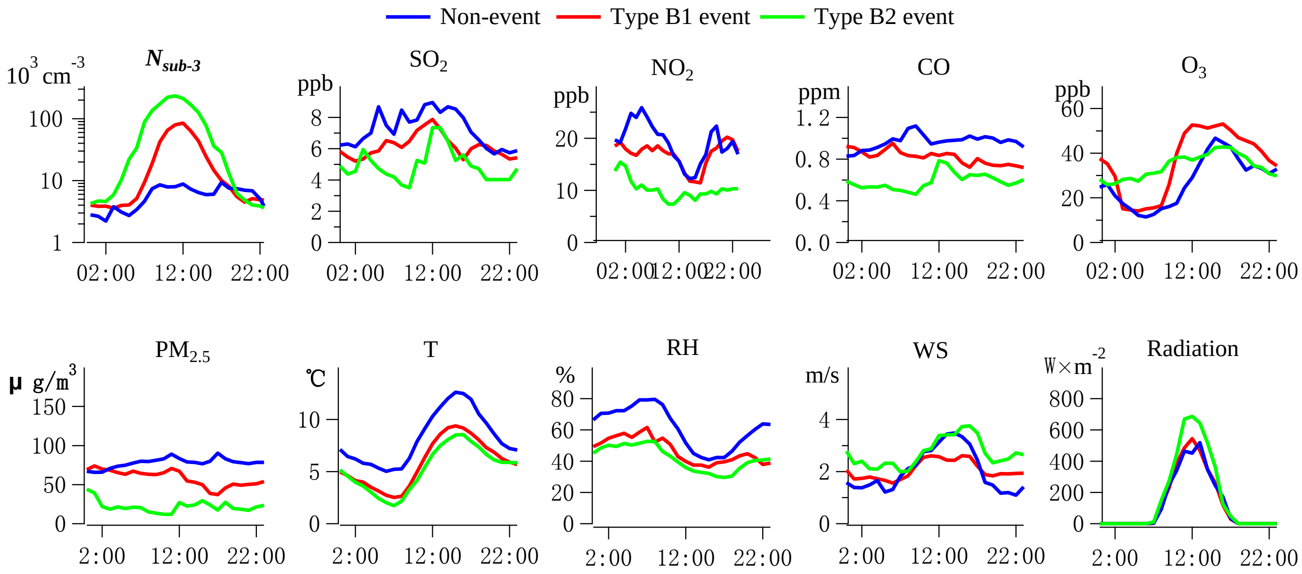

Figure 5. Diurnal variations of mean N_{sub-3}, anthropogenic trace gases (SO$_2$, NO$_2$, CO and O$_3$), PM$_{2.5}$, and meteorological variables (temperature, RH, wind speed, and solar radiation flux) on non-event days (n=8, blue line) and event days (n=3 for Type B1 event, red line and n=6 for Type B2 event, green line) during winter measurement period.

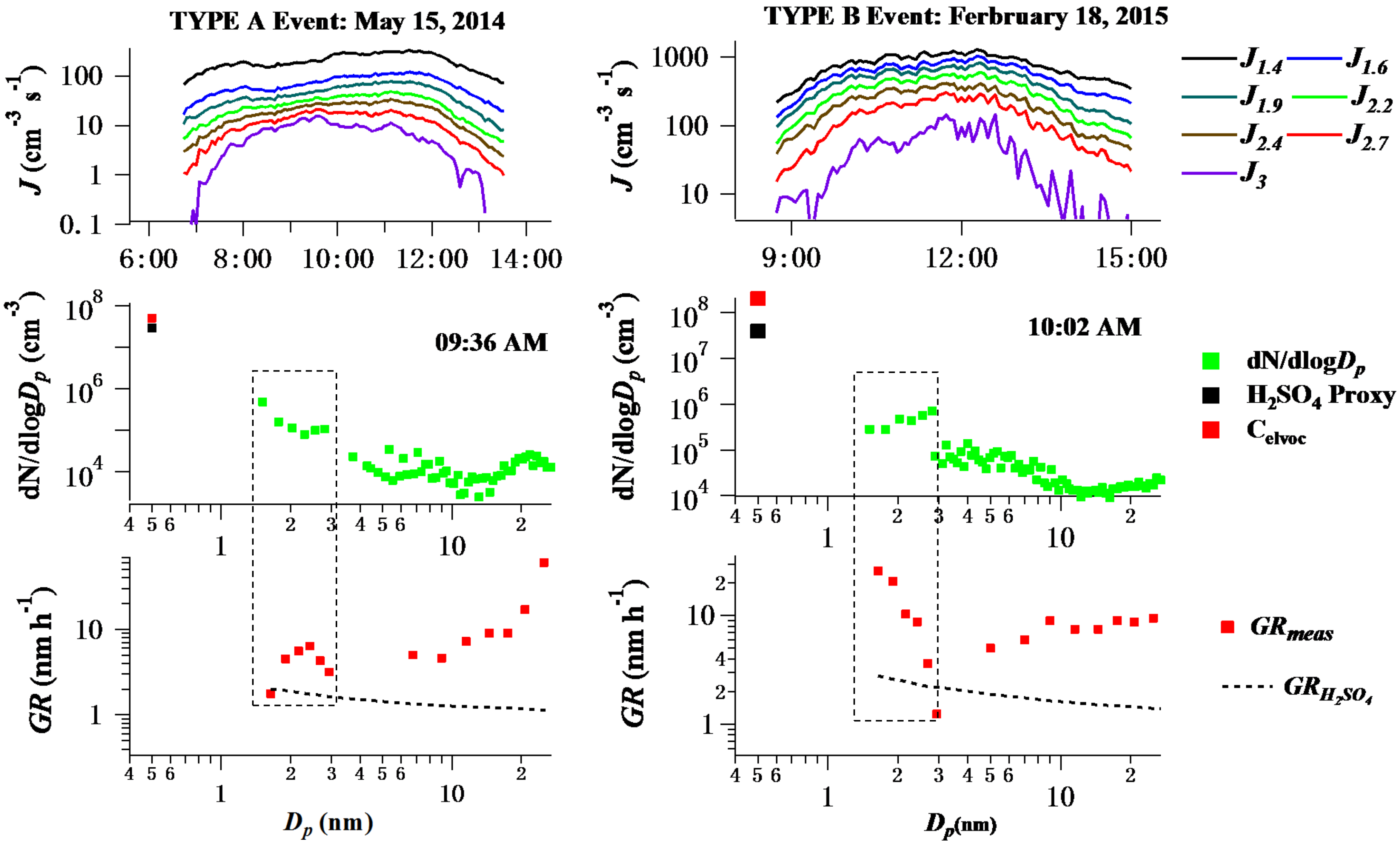
TYPE A Event: May 15, 2014
TYPE B Event: Ferbruary 18, 2015
J (cm-3 s-1)
0. 1
1
10
100
1000
6:00
8:00
10:00
12:00
14:00
9:00
12:00
15:00
J1.4
J1.6
J1.9
J2.2
J2.4
J2.7
J3
dN/dlogDp (cm-3)
09:36 AM
10:02 AM
dN/dlogDp
H2SO4 Proxy
Celvoc
GR (nm h-1)
GRmeas
GRH2SO4
Dp (nm)
Dp(nm)

Figure 6. Upper: formation rates (or equivalently, particle growth fluxes) of 1.4, 1.6, 1.9, 2.2, 2.4, 2.7 and 3.0 nm cluster/particles on May 15 2014 (Type A1 event) and Feb 18 2015 (Type B1 event). Middle: particle size distribution (dN/dlogD_p, green square) selected during the two events (9:36 AM and 10:02 AM). Lower: particle growth rates measured during the same time periods (GR_{meas}, red square). Also shown in the figure were H_2SO_4 proxy (black square) and growth rates calculated from the H_2SO_4 proxy (GR_{H2SO4}, dashed black line), as well as the calculated ELVOC concentration ($\mathrm{C_{elvoc}}$, red square, see Eq.5) during the same time periods. Dashed boxes in the lower panels highlighted the size distributions and growth rates between 1.4 and 3 nm measured with nCNC.

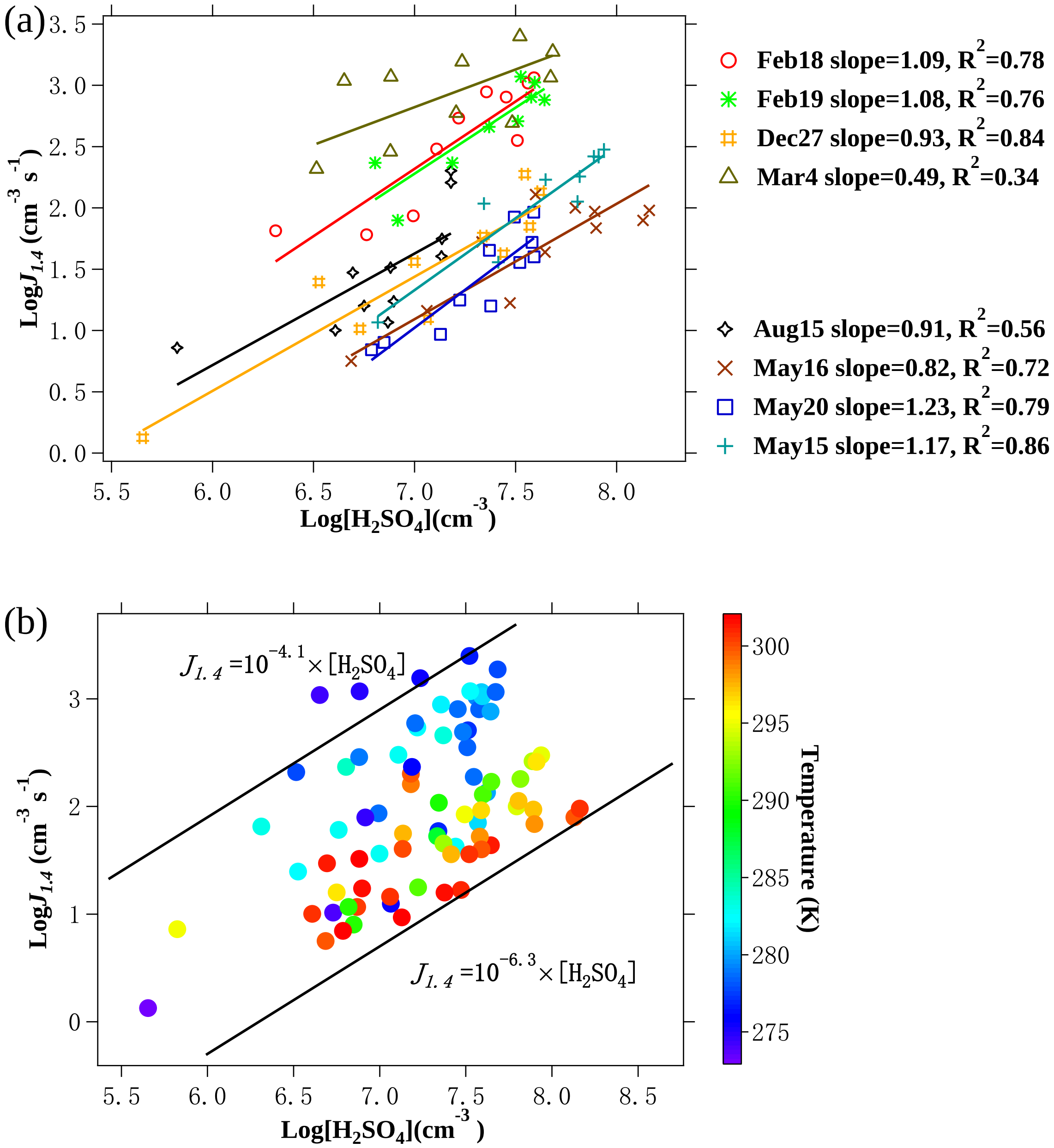

Figure 7. (a) Correlations between log $J_{1.4}$ and log [H_2SO_4] for the 8 events. H_2SO_4 proxy was calculated according to Mikkonen et al. (2011). $J_{1.4}$ and [H_2SO_4] were synchronized to 1 hour that was the time resolution of solar radiation data. The colored lines showed linear fits to the data of every single event. (b) The same dataset as (a), but with symbol color to indicate ambient temperature. Two black lines showed the linear dependences of $J_{1.4}=10^{-4.1} \times [H_2SO_4]$ and $J_{1.4}=10^{-6.3} \times [H_2SO_4]$, between which most of data points located.

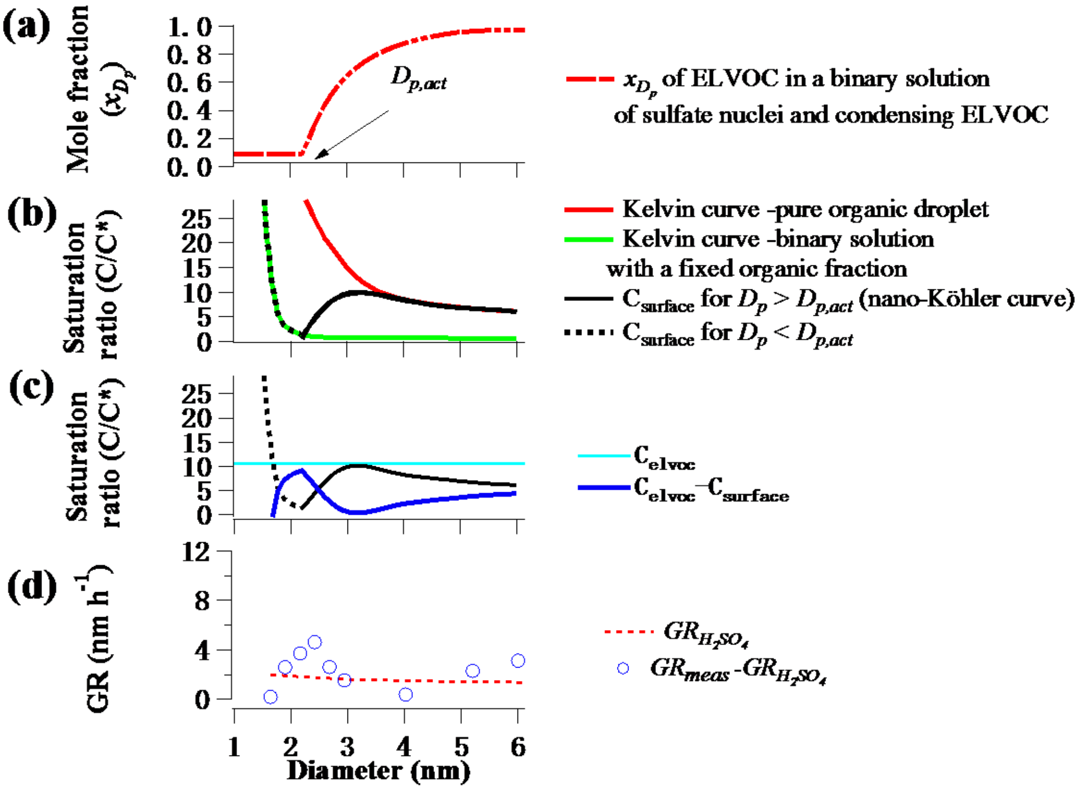

Figure 8. (a) Mole fraction of organics (x_{D_p}) in a binary solution of sulfate nuclei and activating organics (ELVOC) in a new particle. Nuclei activation diameter $D_{p,act}$ is the size where ELVOC begins to dilute the nuclei. (b) Kelvin equilibrium curves over a pure organic droplet (red line) and a binary solution with a fixed organic fraction (green line), nano Köhler curve for $D_p > D_{p,act}$ (black solid line) and surface concentration $C_{surface}$ for $D_p < D_{p,act}$ (black dashed line). (c) gas phase concentration of the organic vapor (C_{elvoc} , cyan line), surface concentration C_∞ (black line), and $C_{elvoc} - C_{surface}$ (blue line). (d) Growth rate GR_{H2SO4} due to H_2SO_4 (Mikkonen et al. 2011 proxy) and growth rate due to organic vapor $GR_{elvoc,meas}$, calculated as GR_{meas}-GR_{H2SO4}.

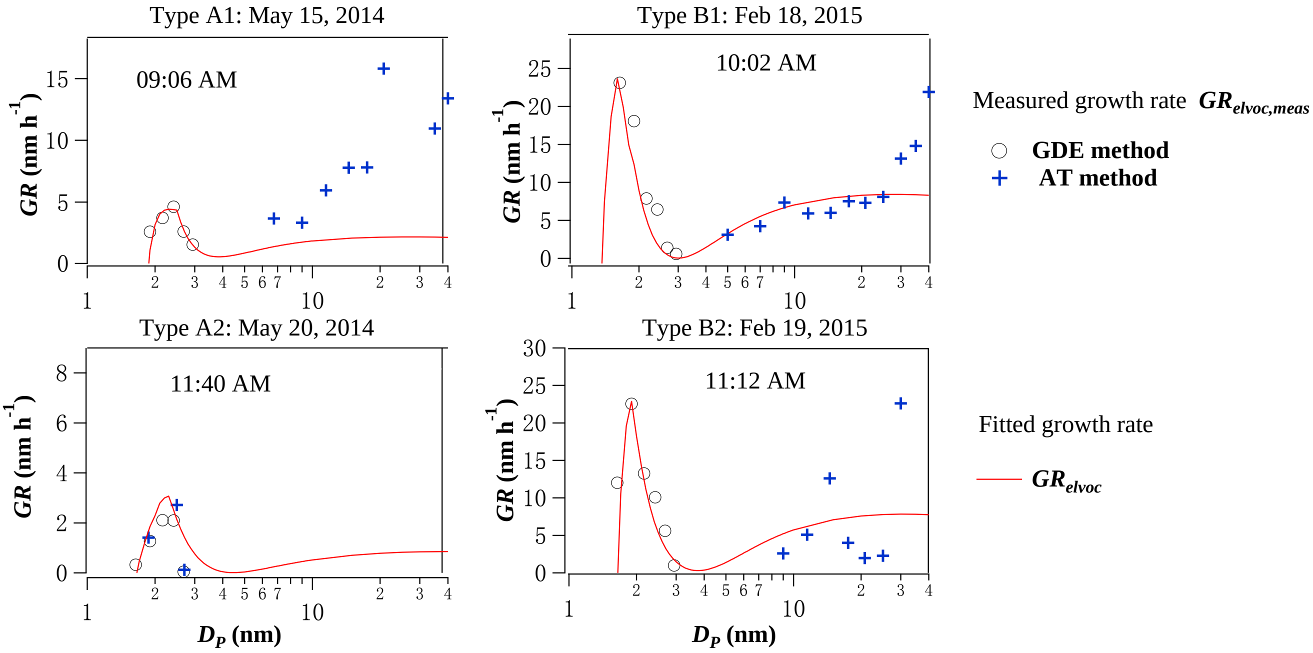

Figure 9. Comparisons of measured ($GR_{elvoc,meas}$, black circle) and fitted (GR_{elvoc}, red line) growth rates from Eq. (4) for typical Type A1, A2, B1, and B2 events. Also shown were growth rates calculated from appearance time method (blue cross) for sub-3 nm particles when growth rate was relatively small or for larger particles with large size intervals.